Mineral and chemostratigraphy of a Toarcian black shale hosting Mn-carbonate microbialites (Úrkút, Hungary)

Márta Polgári[1,2*], James R. Hein[3], Lóránt Bíró[1], Ildikó Gyollai[1], Tibor Németh[1], Sajgó Csanád[1], József Fekete[1], Lorenz Schwark[4], Elemér Pál-Molnár[5], Mária Hámor-Vidó[1], Tamás Vigh[6]

[1] *Research Center for Astronomy and Geosciences, Geobiomineralization and Astrobiological Research Group, Institute for Geology and Geochemistry, Hungarian Academy of Sciences, Budapest, 1112 Budapest, Budaörsi str. 45, Hungary, e-mail: rodokrozit@gmail.com*

[2] *Eszterházy Károly College, Dept. of Natural Geography and Geoinformatics, 3300 Eger, Leányka str. 6, Hungary*

[3] *USGS, 400 Natural Bridges Dr., Santa Cruz,* CA 95060, U.S.A., *jhein@usgs.gov*

[4] *CAU, Kiel, Germany, ls@gpi.uni-kiel.de*

[5] *Szeged University, Dept. of Mineralogy, Geochemistry and Petrology, Egyetem str. 2-6, 6702 Szeged, Hungary, palm@geo.u-szeged.hu*

[6] *Mangán Ltd, Úrkút, Külterület 1. 8409 Hungary, manganvigh@vnet.hu*

**corresponding authors:*

rodokrozit@gmail.com

Abstract: 300 words **Text: 9004** words **Figures: 13 Tables: 5 SI 7**

Abstract

Toarcian black shale that hosts Mn-carbonate microbialites at Úrkút, Hungary was investigated by mineralogical, inorganic, and organic geochemical methods for characterization and comparison with other European black shales representative of the Toarcian Oceanic Anoxic Event. Based on the authigenic mineral composition, calculations were made to estimate environmental conditions during sediment accumulation and early diagenesis. Geochemical and petrographical results of organic, carbonate, and REE multiple-proxy analyses revealed a strong congruence between the host black shale and the Mn-carbonate ore beds. The Úrkút black shale is really a grey shale with moderate to low TOC content that accumulated in a starved basin. The organic matter content and anoxic characteristics resulted from rapid accumulation of microbial organic matter from microbial booms, accompanied by a geothermally generated hydrothermal circulation system, and a high rate of authigenic mineral formation (clay minerals and proto-ore minerals). The inferred enzymatic Mn and Fe oxidation blocked carbonate formation by decreasing the pH. The system remained suboxic via syngenetic mineral accumulation (Fe-rich biomats), and became anoxic during diagenesis in conjunction with pyrite generation. The separation of black shale beds and Mn-ore beds is not distinct through the section. Instead, a distal hydrothermally induced clay-rich authigenic assemblage (marlstone) best describes the black shale, in which Mn-oxide proto-ore beds (Mn-rich laminae) formed from the beginning of black shale deposition, when the oxygen supply in the sedimentary basin was insufficient for enzymatic Mn(II) oxidation. Mn-oxide proto-ore turned into Mn-carbonate ore via microbially mediated processes during early diagenesis. The drivers for Mn-bearing organic matter-rich marlstones were most probably a combination of regional and local processes, with generation of a tectonic rift system that promoted geothermally generated hydrothermal fluids, which initiated microbial blooms. Black shale mineralogy, geochemistry, and organic matter at Úrkút differ from those of the epicontinental shelf black shales of the Tethyan ocean.

Keywords: T-OAE, Mn-carbonate, black shale, multiple proxies, microbial, failed rift, geothermal circulation

Highlights mandatory

Multi-proxy study of the Alpine-Mediterranean black shale was performed.

Mineralogy and geochemistry of the ore and the black shale are very similar.

Ore was formed via microbial blooms governed by hydrothermal activity.

Mineralogical and geochemical data reflect an ancient failed rift system.

Úrkút proxies differ from those of the Tethyan epicontinental shelf occurrences.

1 Introduction

Organic geochemistry of black shales has been widely studied (e.g. Wignall, 1994; Jenkyns, 2010) because of their key role in understanding global changes, for example the Toarcian Ocean Anoxic Event (T-OAE). Black shales are of enormous economic importance because they are source rocks for the bulk of the World's hydrocarbons, and metalliferous black shales form ore deposits for many metals (e.g. Cu, Ni, Pb, V, Mo, Mn), and yet they are among the least understood sedimentary rock. The identification of paleo-oxygen levels is therefore of critical importance in the paleoenvironmental reconstruction and understanding the genesis of black shales (Wignall, 1994).

In the early Toarcian, global environmental change caused considerable mass extinction of terrestrial and marine organisms (Jenkyns, 1985, 1988; Pálfy and Smith, 2000; Pálfy et al., 2002). At the same time, a ~5-7‰ negative $\delta^{13}C$ excursion of carbon reservoirs was identified (marine organic matter, marine carbonate, terrestrial plants), as well as an abrupt increase of ocean water temperature has been identified (Küspert, 1982; Jenkyns and Clayton, 1997; Hesselbo et al., 2000; Rosales et al., 2004; Kemp et al., 2005). As a consequence of global, regional, and local effects, the accumulation of organic material increased resulting in a global distribution of black shales (Jenkyns, 1985, 1988; Haas, 2012).

For interpretation of the enriched organic matter accumulation and the negative $\delta^{13}C$ excursion, models were established. Among those models, some important global and local ones include: (i) Volcanic activity (Karoo-Ferrar continental plateau basalt formation) as a global catastrophe was the driving force for climate change that triggered black shale deposition. The global response to considerable volcanic CO_2 emission resulted in changes of sea level and current systems, which led to increased biomass productivity in upwelling zones (Jenkyns, 1985, 1988; Jenkyns and Clayton, 1997; Vető et al., 1997; Pálfy and Smith, 2000; Röhl et al., 2001;

Schmid-Röhl et al., 2002; McArthur et al., 2008). (ii) Massive dissociation of methane hydrates caused by the warm climate was also proposed (Hesselbo et al., 2000; Kemp et al., 2005). (iii) Water stratification in silled basins may have obstructed oxygen supply, a local process without invoking global drivers (e.g., salinity differences, Röhl et al., 2001; Schmid-Röhl et al., 2002; Schwark and Frimmel, 2004; van de Schootbrugge et al., 2005). (iv) Mixed scenarios of global events, e.g. reduced levels of atmospheric oxygen and global ocean changes (Hallam, 1967, 1981). Early Toarcian black shales occur worldwide, although their onset and decline are potentially diachronous (Wignall et al., 2005). Understanding the conditions of formation and paleoenvironments of the black shales is important; clarification of global, regional, and local drivers is a great challenge (Haas, 2012).

Two types of lower Toarcian black shales of the western Tethyan Ocean can be distinguished (Jenkyns, 1985, 1988): (i) accumulation on an epicontinental shelf [(boreal, Jet Rock, Great Britain (Sælen et al., 2000); Schistes Cartons, Paris Basin, France (Hollander et al., 1991; Katz, 1994); Posidonia Shale, Germany (Röhl et al., 2001); Lusitanian Basin, Portugal (Jenkyns, 1985, 1988; Duarte, 1998)] and (ii) Alpine-Mediterranean Tethyan Region [(Umbria-Marche Basin, Italy (Jenkyns,1985, 1988; Duarte,1998); Úrkút Basin, Hungary (Polgári, 1993; Vető et al., 1997; Polgári et al., 2012a)]. The boreal type occurs as shallow-water shelf sediments 15-30 m thick, with 5-15 wt. % TOC and a Hydrogen Index (HI) of 300-600 mg HC/g TOC. The Alpine Mediterranean type occurs in pelagic limestone, in rifted areas of Atlantic-type continental margins, with TOC between 1-3 wt. % (up to 10 wt. %), and a generally low HI, 200-300 mg HC/g TOC (Jenkyns, 1985, 1988). Transitional types exist, which show mixed features [(Mecsek Réka Valley Óbánya Siltstone Formation (MRV-ÓSF), Hungary (Varga et al., 2007; Raucsik and Varga, 2008a); Basque-Cantabrian Basin, northern Spain (Rosales et al., 2004)]

(Fig. 1). Besides these typical Toarcian black shales, another classification differentiates between the pure non-ore bearing and an ore-bearing, namely Mn-carbonate types.

Sedimentary Mn deposits have a wide distribution in time and space (Roy, 1981). Their formation extends through more than half of geological history and they are extensively distributed both in the geological record on the continents and on the bottom of the present-day oceans, shallow seas, and lakes. The Jurassic (Toarcian) was an important time of Mn-carbonate mineralization and different ideas about the controls on deposit formation have been put forward, including tectonic activity, volcanism, climatic variations, and combinations of these. Mn-carbonate deposits are typically associated with organic carbon-rich beds (Roy, 1981). Black shale-hosted Mn-carbonate deposits are numerous and most deposits have large reserves of manganese ore with grades of 20-30 wt. % Mn. Numerous subeconomic black shale-hosted Mn deposits occur along with the giant Úrkút deposit in the Alpine-Mediterranean Tethyan Realm (Transdanubian Range: TR) **(**Jenkyns, 1988; Jenkyns et al., 1991). Stratiform black shale-hosted Mn-carbonate deposits reached maximum development during the Toarcian *tenuicostatum-falciferum* ammonite zones in the Strubberg and Allgäu deposits of the Northern Calcareous Alps and Eastern Alps, the Úrkút deposit in the TR of the Southern Alps, in the Tatra unit, and lower Carpathians (Polgári et al., 2012a and references therein).

At different locations, the black shale-Mn associations show similarities and differences: (1) contemporaneous oxic deposits formed under similar environmental conditions occur in some locations (Jenkyns, 1988); (2) not all black shale sections are enriched in manganese (Jenkyns, 1988; Jenkyns et al., 1991, 2001); (3) if they are Mn-rich, the TOC content is relatively low, only 4-5 wt. %, which may support a microbial origin for the Mn-carbonate deposits (Jenkyns, 1988; Polgári et al., 2012a); (4) negative δ^{13}C values of early diagenetic $MnCO_3$ support a contribution from organic carbon to the dissolved carbon reservoir (Polgári et al., 1991); (5) Mn(IV, III) oxides characterized the proto-ore because initial metal enrichment took place in an oxic seafloor environment (Polgari, 2012a). This oxic depositional environment contrasts with the generally accepted explanation for the formation of a laminated black shale, assumed to result from very limited benthic infauna. (6) High primary productivity occurred during black shale deposition (Jenkyns, 1988; Jenkyns et al., 1991, 2001, 2010; Vető et al., 1997) and biomarker studies indicate that organic matter in all these lower Toarcian black shales is dominantly of marine origin, derived from algal and bacterial sources (Farrimond et al., 1989; Polgári et al., 1992; Polgári, 1993; Jenkyns et al., 2001). (7) Formation of $MnCO_3$ immediately pre-dated deposition of the TOC-rich shales in the majority of localities suggesting that their deposition was charactertistic of environmental conditions immediately preceding the anoxic event (Jenkyns et al., 1991). (8) Black shale formation was structurally confined to rifted continental margins of the developing Tethyan Ocean (Bernoulli & Jenkyns, 1974; Channel et al., 1992). Wignall (1994) stressed the possibility that abundant organic carbon deposition overwhelmed the benthos, thereby promoting formation of laminae even with oxic bottom waters.

Diagenetic processes overprinted the seabed manganese depositional signals and caused significant transformations, such as formation of early diagenetic rhodochrosite. The large mass of bacteria living in and on the surface of the sediment provided a large pool of reactive organic matter after death that promoted a series of diagenetic reactions. During decomposition, the consumption of the organic matter by other microbial consortia may have played a key role in diagenesis (via formation of the Mn-carbonate ore). Those anaerobic bacterial cycles were different from the syndepositional aerobic bacterial cycle, although both occurred contemporaneously at different depths in the sediment column.

The black shale-hosted stratiform Mn-carbonate deposits were reported to have mainly a hydrothermal metal source and microbial processes were reported to have occurred in some of the deposits (Cornelius & Plöchinger, 1952; Gruss, 1956; Polák, 1957; Andrusov, 1965; Germann & Waldvogel, 1971; Germann, 1971; Bernoulli & Jenkyns, 1974; Faupl et al., 1982; Beran et al., 1983; Jenkyns, 1988; Krainer et al., 1994; Krajewsky et al., 2001; Rantitsch et al., 2003; Polgári et al., 2012ab). During the past 100 years, numerous studies have addressed the complex formation of the Jurassic black shale-hosted Mn-carbonate ore at Úrkút. The ore beds are now thought to have resulted from a two-step, microbially mediated process that produced a microbialite (Polgári et al., 2012ab, 2013a, 2016). This important deposit is among the 10 largest Mn deposits in its type with current reserves of 80 million tons of Mn-carbonate ore (24 wt. % average Mn and 10 wt. % Fe). The original deposit was much larger, a real giant, hosting about 300 million tons of ore, but much of it was eroded during the Cretaceous and Eocene (Szabó & Grasselly, 1980). The original features of the deposit were overprinted only by diagenesis, and have remained unaffected by significant thermal maturation. The ore deposit and its host black shale have been related to the T-OAE.

Application of models for understanding ancient Mn-carbonates hosted in black shale is difficult, even for unmetamorphosed deposits, because of overprinting of different microbially mediated early-diagenetic processes that took place. The effect is as yet unclear with respect to the role of the black shale host rock, the nature of the contained organic matter, the types of microbiota involved in the primary productivity and the nutrient cycle that supported it, and what microbiota were responsible for aiding the accumulation of huge quantities of metals. These are important questions not only from a scientific point of view but can also contribute to identifying guides for mineral deposit exploration. The age of the Úrkút black shale coincides with the T-OAE and comparison of this black shale to other Toarcian black shales and environments of formation is essential to addressing these questions.

The well-preserved, unmetamorphosed black shale that hosts Mn-carbonate deposits of the Úrkút Basin (Fig. 2abc) offers an excellent case study for detailed petrographic, mineralogical, geochemical, and textural analyses. We have completed mineralogical and chemcial analysis, Rock-Eval pyrolysis, and stable isotope analysis to study basic inorganic and organic geochemical features (kerogen type, maturity, organic petrology). We compare the results with the data available in the literature, focusing on the black shale from the lower part of the MRV-ÓSF Hungary (Varga et al., 2007) and former data from Úrkút (Polgári et al., 1991, 1992, 2000). We also include the data from the Mn-ore sections (Vető et al., 1997).

This paper reviews the main characteristics of the black shale that hosts the Úrkút Mn deposit (Alpine-Mediterranean Tethyan Region), provides additional microtextural, mineralogical and geochemical evidence for the fundamental processes of its formation and its relation to the ore beds, discusses the importance of such deposits in developing paleoenvironmental indicators, provides a new general model for the origin of this type of black shale deposit, and discusses the importance of deposit characteristics for the interpretation of deposit genesis in the framework of the T-OAE.

2. Geological setting

The TR of Hungary is an important region for a series of structurally controlled Jurassic black shales and their associated Mn mineralization. The Úrkút black shale is located in the central part of the Bakony Mountains, which belong tectonically to the North Pannonian unit of the Alps-Carpathians-Pannonian regions (ALCAPA, Fig. 2ab). The largest Mn deposits occur in the Úrkút basin and at Eplény, which formed by the NW-SE trending block faulting that characterized the Late Triassic and Jurassic of this region (Fig. 2b). These deposits are within marine sedimentary rocks composed mainly of bioclastic limestone, radiolarian clayey marlstone, and dark-grey to black shale (Polgári, 1993). Smaller, similar types of deposits occur along fault zones parallel to the largest deposits.

The Úrkút Mn mineralization occurs in two main units in the 40 m thick section (Fig. 3, SI. 1). (1) Cherty, Fe-rich, primary Sr-bearing Mn-oxide mineralization occurs in varicolored metalliferous claystones that overlie strongly leached limestone. The deposit is composed of blocks, nodules, and wad beds in close proximity to fracture zones oriented N-NW–S-SE along the NE-SW trending unit of approximately 12 km length and 4-6 km width (Úrkút-Csárdahegy and Eplény, Polgári et al., 2012a). Currently, the extent of the ore deposit of economic importance is about 8 km^2.

The black shale (clayey marlstone)-hosted Mn mineralization (2) is Toarcian (*falciferum* ammonite zone; Géczy, 1973). The marlstone rests conformably on middle Lias carbonate rocks. Mn mineralization is restricted to two main intervals within the marlstone, separated by black shale units (Bs1, Bs2, Bs3-4, Fig. 3, 4, SI. 2). The lower first (main) ore bed is about 8-12 m thick. The base of the first ore bed begins with 0.5 to 1 m thick black shale (Bs1), which is greenish, organic-rich, pyritiferous, containing enrichments of trace elements, Co, Ni, Cu in high As-bearing sulphides, and Sr-bearing barite (Polgári, 1993; Polgári et al., 2003a). Concretions and thin layers of phosphate and chert are common at the boundary of the marlstone and the underlying limestone (Polgári et al., 2003b; 2013b). The upper mineralized zone (second ore bed) is 2 to 4 m thick and is separated from the first ore bed by 10 to 25 m of black shale (Bs2). The second ore bed can interfinger with black shale (Bs3-4). The Ca-rhodochrosite ore is composed of alternating grey, green, brown, and black sections of finely laminated, very fine-grained clay mineral carbonate mixtures (Cseh Németh et al., 1980). Fine-grained (1-2 μm) rhodochrosite rock lacks coarse detritus and is laminated (Szabó Drubina, 1959). Mineralized sections lack fossils including benthic trace fossils, and only rarely contain fish remnants as well as silicified, Mn-replaced, or coalified plant fragments (Polgári et al., 2005). The ore body formed in a structurally controlled marine basin via bacterial enrichment of Mn and bacterially mediated, early diagenetic formation of Mn carbonates. It has been proposed that hydrothermal fluids venting into the depositional basin were involved in the mineralization (Polgári et al., 2012a). The Fe and Mn oxides were probably deposited from deep-sourced fluids circulating through basement rocks. Circulation along zones of structural weakness was likely driven by high geothermal gradients (Polgári et al., 2004; 2007, 2012a).

The history of development of the Mesozoic TR in the ALCAPA was determined from its paleogeographic position in the Tethyan system. The Transdanubian terrane, part of the Tethyan shelf, was located between the Southern Alps and the Upper Austro-Alpian nappes during the complex development of the Mesozoic ocean (Fig. 2c). Its initial displacement started during the Eocene by way of NE lateral motion and it arrived at its present location in the early Miocene (Kázmér & Kovács, 1985; Csontos & Vörös, 2004). A Middle Jurassic paleogeographic map (Haas, 1994) shows that the input of terrestrial detritus was blocked by the Ligur-Pennine Ocean and the Neotethys (Fig. 2c). Continental volcanic activity and oceanic spreading centers were widespread in the Neotethys and Ligurian-Penninic Oceans.

1. Samples and methods

Oriented samples (n=19) were collected through the entire black shale sections hosting the Mn-ore beds (Table 1, SI. 1). Besides the new collection (n=19, FP series, Fig. 3), previously collected samples were also taken into consideration (n=12). Bulk and individual lamina sub-samples were examined to determine macroscopic features (FP series Fig. 4, SI 2). FP3-FP11 are not oriented samples. Petrographic structural-textural studies were made on 14 oriented thin sections in transmitted light (NIKON ECLIPSE 600 rock microscope, IGG, HAS, Budapest).

X-ray powder diffraction of 50 samples including subsamples for mineralogy was done using a Philips X-ray diffractometer (PW 1710) with carbon monochromator and Cu Kα radiation. Mineral composition was determined on randomly oriented powdered samples by semi-quantitative phase analysis according to the modified method of Bárdossy et al. (1980), using previously defined intensity factors.

Black shale samples were analysed for chemical and mineralogical contents (n=30, sub-samples were the following: FP16, FP16A, FP16B (A-lower part; B-upper part of samples, B1-lower part; B2-upper part of samples), FP23A, FP23B1, FP23B2, FP25A,B.) The samples were analyzed for 40 major, minor, and trace elements using 4-acid digestion (hydrochloric, hydrofluoric, nitric, perchloric acids) in conjunction with inductively coupled plasma-atomic emission spectrometry (ICP-AES) and ICP-mass spectrometry (ICP-MS; SGS Laboratories, Ottawa, Canada). The resulting solutions were taken to dryness and the residue dissolved with 1 ml of aqua regia and then diluted to 10.0 g with 1% (volume/volume) nitric acid. Another split of each sample was fused with lithium metaborate then analyzed by X-ray fluoressence after acid dissolution of the fusion disk. This technique, provides analysis of all major elements, including Si, and a few minor and trace elements. The accuracy of Si determinations was good, about 2-4% based on the total-oxide sums, even for high-Si cherts. Sr and Ba contents were determined by both the 4-acid digestion and fused disc techniques, which produced comparable results. Titanium and Cr were also analyzed using both techniques, but only data from the fused-disc technique are used because the fusion technique more completely digests refractory minerals that might contain those elements.

Se, Te, As, Sb, and Tl concentrations were determined using hydride generation followed by atomic absorption spectrometry (AAS). Mercury was determined by cold vapor AAS.

Preliminary information of the major contributors to OM content were determined by Rock-Eval analysis (n=27). Rock-Eval measurements were carried out at the University of Kiel, using VINCI Rock Eval II Plus instrument following established protocols (Espitalie et al., 1985).

Maceral analysis at reflected white light and excited blue light observation supported the organic matter studies on ground whole-rock samples embedded in epoxy resin and polished according to ISO7404-2 standard. Maceral analysis and vitrinite reflectance measurements followed the method of Taylor et al. (1998). In our study, the main ore bed and the overlying black shale Bs2 zones were sampled and analyzed with 14 samples. Maceral analysis was carried out not only on marly shales but also five ore samples were selected with green and brownish grey colors of the finely laminated Mn carbonates of the main ore bed.

Organic carbon isotopic compositions were measured after decarbonation using a Finnigan Delta V continuous-flow mass spectrometer equipped with a Thermo Flash elemental analyser (IGG, HAS, Budapest) (n=29). Standard deviation of the data is below 0.1‰ based on the reproducibility of sample and laboratory standard data. $\delta^{13}C_{VPDB}$ and $\delta^{18}O_{SMOW}$ data were measured for carbonates (n=27).

IR measurements were done using a Bruker VERTEX 70 Fourier transform infrared spectrometer equipped with a Bruker Hyperion 2000 microscope with 20x ATR objective and MCT-A detector (IGG, HAS, Budapest) (n=2). During ATR analysis, samples were contacted with the tip of the Ge crystal (0.5 micron) on selected 1 N pressure. The measurements were conducted for 32 seconds in the 600-4000 cm-1 range with 4 cm^{-1} resolution. Opus 5.5 software was used to evaluate the data. Contamination of epoxy glue and glass were taken into consideration, and peaks of these phases were not considered.

4. Results

4.1. Bulk mineralogy (XRD)

The black shale minerals are typically microcrystalline, averaging 1–2 μm in size, with very rare detrital mineral grains up to several tens of micrometers in diameter (e.g. quartz, feldspar). Black shale mineralogy and mineral genesis, grouped by mineral types, are summarized in Table 2. The mineral distribution varies among and within each of the black shale sections (Fig. 5). The mineral assemblage is similar to that of the ore beds but the minerals occur in different proportions. The bulk mineralogical composition of the black shale consists of (i) carbonates (calcite, dolomite, rhodochrosite kutnohorite and siderite); (ii) oxides (quartz); (iii) silicates – clays (smectite, celadonite, chlorite and kaolinite), K-feldspar, plagioclase and zeolite; (iv) sulfides (pyrite); (v) and sulphates (gypsum, barite).

The black shale is dominated by authigenic clay minerals such as smectite and celadonite, as well as quartz, but in some sections the content of dolomite, K-feldspar, and plagioclase increses moderately. Calcite is also enriched in some laminae. Rhodochrosite-rich laminae first occur very close (few cm) to the contact zone of the footwall in the black shale Bs1 (Fig. 5). Pyrite occurs commonly in the black shale sections. The second ore bed is characterized by alternating thin ore and black shale layers, which are macroscopically not distinguisable. Other minerals occur as trace components.

4.2. Rock microscopy

Thin section observations show a representative series of partly pyritized Fe-rich biomats occurring as brown goethitic finely woven microtextures in a fine-grained matrix (Fig. 6a-h, SI. 3). This typical texture occurs from the bottom to the top of the sections. Fish debris composed of apatite is very common in the samples (Fig. 6dh). Carbonate biodebris and other mineral clasts (quartz) are enriched in distinct intervals, or occur randomly. The fine-grained matrix is carbonate-bearing and clay-mineral rich.

4.3. FTIR

Determination of goethite and apatite was made by FTIR from thin sections, which verified the presence of these minerals (Table 2).

FP16A and FP22A samples both contain iron oxides with clay minerals and carbonates (SI. 4). The infrared spectra were taken on fine-grained patches with reddish-brown material in transmitted light. The iron oxides were determined after Glotch and Rossman (2009). The infrared spectra of FP16A and FP22A contain Fe-O vibration of akaganéite (665 cm^{-1}), goethite (667 cm^{-1}, 805 cm^{-1}), and maghemite (730 cm^{-1}).

The characteristic infrared vibrations of clay minerals were identified after Madejová and Komadel (2001). Sample FP16A contains a mixture of kaolinite and smectite with peaks at 680 cm^{-1} (Si-O perpendicular stretching), 846 cm^{-1} (AlMgOH deformation), 1005 cm^{-1} (in-plane Si-O stretching), 3637 cm^{-1} (OH stretching of structural hydroxy groups), and 3734 (Si-OH bending of adsorbed water). Sample FP22A contains mostly smectite with characteristic peaks at 688 cm^{-1}, 841 cm^{-1}, 1011 cm^{-1}, 3573 cm^{-1} (bending of structural OH groups), and 3623 cm^{-1}.

The infrared molecular vibrations for carbonate were interpreted after Müller et al. (2014), which occur in both the FP16A and FP22A samples. The FP16A has CO_3 peaks at 864 cm^{-1} and 1397 cm^{-1}, the C-O vibrations at 2343 and 2365 cm^{-1}. Sample FP22A contains only

CO_3 bands of carbonate at 864 cm-1 and 1400 cm-1. Organic material and hydroxyapatite was identified only in sample FP22A.

The organic material was identified after Parikh and Chorover (2006). The band at 1526 cm^{-1} is attributed to C-N and C-H deformation, the band at 1705 cm^{-1} to C-O and C-H vibrations. Both of the above mentioned peaks are characteristic for amides, which may originate from biogenic material.

The infrared peaks of apatite were identified following Figureido et al. (2012), with structural PO_4 vibrations at 872 cm^{-1} and 1012 cm^{-1}.

4.4. Chemistry

Chemical compositions are summarized in SI. 5 and 6, and based on those data, paleoenvironmental proxies were calculated (Table 3A).

The Úrkút black shale has average contents of 18.2 wt. % Si (max: 26.98 wt. %), 3.7 wt. % Al (max: 6.2 wt. %), 6.9 wt. % Fe (max: 17.3), 5.7 wt. % Mn (max: 20.9), and 5.3 wt. % Ca (max: 10.6). The concentration of S is 2.0 wt. % on average (max: 4.5), which reflects the high pyrite content of the black shale. Other components on average are below 1 wt. %, but the maximum P content reaches 2.8 wt. %. Co shows some enrichment in pyrite and Sr is enriched in barite; Ba averages 307 ppm, with a maximum of 3020 ppm (Polgári et al., 2003a). Co, Ni, As, and REE enrichments are related to disseminated grains a few tens of micrometers in size, e.g., Co-, Ni-, Ag-sulfide, and Co- and Ni-bearing pyrite, which are mainly in the black shale underlying the main carbonate ore bed (Bs1).

Enrichment factors (EF) of elements in the black shales compared to Average Shale (Wedepohl, 1971) show a mean for Mn of 7.2, Fe of 2.5, and P of 3.7, while the mean S content shows a high EF (11.7). V (average: 100 ppm; max: 183 ppm), Mo (av: 7.9 ppm; max: 15 ppm), and Cr are depleted in the black shale relative to average shale. Ni is near crustal abundance, although Cu has an EF in the black shale of 3.

4.5. Organic geochemistry and petrology

Total organic carbon (TOC) values in Bs1 range between 0.59% and 1.06 wt. % (mean 0.84%), in Bs2 between 0.56% and 3.53 wt. % (mean 2.08%), and in Bs3-4 between 0.61% and 1.73 wt. % (mean 1.12%) (Table 4). TOC correlates with N content reflecting the organic origin of N. C/N ratios scatter around 20, and in Bs1 it ranges between 14 and 21 (with one outlier value of 31.5), in Bs2 C/N ratios range between 14 and 27, and in Bs3-4 between 17 and 23, showing relatively higher values in Bs2. Carbon isotopic composition of organic matter in Bs1 varies from –30.5‰ to –33.6‰ (VPDB), in Bs2 it from –31.8‰ to –32.9‰ (VPDB), and in Bs3-4 from –29.9‰ to –30.8‰ (VPDB). Bs2 shows less negative carbonate δ^{13}C (–2.8‰ to –18.1‰ VPDB) and more negative δ^{18}O values (–1.7‰ to –4.1‰ SMOW) compared to Bs1 (δ^{13}C: –5.1‰ to –9.8‰ VPDB); δ^{18}O: +0.9‰ to –1.8‰ SMOW) and Bs3-4 (δ^{13}C: –4.0‰ to –10.0‰ VPDB); δ^{18}O: –0.6‰ to –2.8‰ SMOW). Hydrogen Index (HI) values indicate algal contributions (Type-II kerogen) in Bs2, while Bs1 and Bs3-4 samples are characterised by values representative for oxidized organic matter or Type-III kerogen. HI (and correlation with TOC) values are generally higher in Bs2 (87 – 490 mgHC/gTOC) than in the other sections (41 - 106 and 55 - 172 mgHC/gTOC for Bs1 and Bs3-4, respectively). The values in the second ore bed are not lower than in Bs1 and Bs3-4. The δ^{13}C values of organic matter (OM) show a tendency towards less negative values up through the whole section, and a slight positive shift in the first ore bed (main ore bed).

S1 values are below 0.5mgCH/g rock in all samples, while S2 values are above 3 mgCH/g rock are only found in the upper part of Bs2, and fall below 5, generally below 2.5 (fair and poor source rock, respectively). T_{max} is below 435°C in all black shale sections and does not show stratigraphic trends. All the samples are in the early stage of diagenesis.

TOC%, N%, C/N, S1, S2, and HI values show an increasing trend towards the inner parts (between 12.25 - 17.70 m) of Bs2. That depth interval could not be sampled in the mine due to the lack of access. However, the inclusion of data from Vető et al. (1997; see Discussion) documents the lack of any trends through that interval.

The average vitrinite reflectance is 0.3%. The black shale samples are generally rich in liptinite, where weak brownish fluorescing and non-fluorescing bituminite and liptodetrinite of solitary alga are the major constituents, 45-95% of the OM (SI. 7). The occurrence of vitrinite and inertinite of terrestrial origin is subordinant through the entire profile. The occurrence of vitrinite particles is the highest in the main ore bed, with 5 μm size that ranges from 5% to 50% in relative volume from the lower 0.85 m to 3 m distance from the underlying limestone. The size of vitrinite particles increases in the Bs2 to 50-100 μm at the top and their relative contribution to the OM decreases in the middle part of the unit because liptinites became more abundant here in accord with the TOC% and elevated HI. Inertinite content is usually below 5% with the exception of the lowest sample of the main ore bed. Primary, morphologically recognizable liptinites are represented by telalginite, tasmanites type alginite and liptodetrinite of planktonic origin and 1-3 μm in size through the entire section. Laminated alginite makes up 10-12% of the alginite but due to intense degradation their longer diameter is often limited to 20-50 μm. Telalginites most likely have the highest frequency occurrences in the ore layers compared to the Bs2. This may be due to the higher resistance of exin cell walls to bacterial decomposition, and to the in situ oxidation during mineralization and precipitation of Mn and Fe with the consumption of the less resistant bituminite, laminated alginite, and liptodetrinite.

The bituminite content is the highest in the black shale with flaser texture at 500 times magnification. Non-fluorescing bituminite is subordinant in the main ore bed, but its structure and appearance is similar to that observed in the Bs2-like biomats. The texture of the samples of the main ore bed shows similarities to the Bs2 samples.

Chitinite occurres in the Bs2 zone, but the other zooclasts like fish bone particles are present in the main ore bed.

5. Discussion

Huge black shale-hosted Mn-carbonate deposits offer a special opportunity for determining paleo-oxygen levels. Low-temperature aqueous Mn(II) oxidation takes place via bacterial activity by a two-step enzymatic process that requires oxidative conditions (Tebo et al., 2004; Webb et al., 2005; Bargar et al., 2005) during accumulation of the Mn(IV, III) oxide proto-ore. Black shale formation in the Úrkút basin was likely the result of moderate productivity (Table 3A) caused by bacterially mediated reactions and plankton productivity, which upon burial underwent decomposition of the reactive marine organic matter via Mn(III, IV) reduction. The high productivity proposed by Vető (1993), Vető et al. (1995), and others may have inhibited the colonization of the basin by benthic infauna, even under moderate upwelling conditions. However, as indicated by our data, lamination and the lack of benthic fauna occurred even with oxic bottom waters and moderate primary productivity. Vető (1993) also concluded that the Úrkút basin in the early Toarcian sea did not contain H_2S and had oxic bottom waters, which is supported also by the size distribution of framboidal pyrite (Polgári et al., 2016).

5.1. Chemical composition and multi-proxy paleoenvironmental geochemistry

Chemical, enviromental. and genetic proxies indicate formation of the black shale under oxic to sub-oxic bottom-water conditions, high to moderate surface-water productivity, typical marine conditions, low terrigenous input, and no direct hydrothermal input. The proxies for the black shale sections Bs1, 2, 3-4 and the Mn-carbonate ore beds show strong similarities (Table 3A). The Úrkút black shale formed predominantly under suboxic bottom-water conditions and experienced anoxia only during early diagenesis, by microbially mediated sulphate reduction and pyrite formation (Polgári et al., 2016).

Neuendorf et al. (2005, p. 72) described black shale as a laminated, organic-rich shale with 5% or more carbon content that also contains sulfides (usually pyrite) and elevated concentrations of some elements, e.g. U, V, Cu, Ni. Though the Úrkút black shale is laminated and contains sulfides (pyrite), its organic carbon content is lower than 5% and it is depleted in V, U, and Ni. The EF of Cu is only 3. Based on bioproductivity proxies (P, Ba) and redox elements like Cr, Co, Ni, Cu and Pb, the MRV-ÓSF sites were enriched, which is similar for the Úrkút shale, except for Cr, Ni and Pb (Raucsik & Merényi, 2000).

Kearey (2001, p. 30) gave a similar definition for black shales based on organic matter content and indicated that they generally formed under anoxic marine bottom-water conditions. This definition does not fit the Úrkút depositional environment, where the black shale sediment was deposited under oxic bottom waters (Polgári et al., 2013a, 2016). The organic matter content of T-OAE black shales is highly variable, but often below 2 wt. % (Jenkyns, 1988). Jenkyns (1988) emphasized that the Mn-rich black shales contain much less organic matter (around 5 wt. %), than the metal-free black shales. It is essential to distinguish ore-bearing and non-ore-bearing black shales and to further distinguish sulfidic ore-bearing and Mn-carbonate ore-bearing black shales, because their redox and other environmental conditions were different. The Úrkút black shale generally follows the observations of Jenkyns (1988), but has even less organic matter

(Table 4) than he indicated, and does not fit with the idea of anoxic marine bottom waters (Table 3A).

Most of the Toarcian black shales have been studied for organic compounds but inorganic geochemical data are scarce, which does not allow for detailed comparisons. Enrichment factors >5 for the Posidonia Shale occurs only for S and Sc with a maximum for S of 11.5, whereas for the Úrkút Shale, the enriched group of elements is much greater (Te, Co, S, As, Mn, Mo, Ca) (Table 3B), with a maxima for Co (15.0) and Te (17.4) (João et al., 2012). The elements depleted relative to average shale are In, Hf, K, Ba, and Na for the Úrkút black shales, which compares with the Posidonia Shale for K, Na and Ba, but not for Sb, Rb, Ti, Zr, Mg, Mn, which are depleted in Posidonia Shale.

Paleoproxy redox indicators (Ni/Co, V/Cr, V/V+Ni), Mn*=log [(Mn/Mn_{PAAS})/(Fe/Fe_{PAAS})]; Taylor and McLennan, 1995) indicate oxic conditions for the Úrkút depositional basin. However, results of paleoredox indicator element ratios must be used with caution because of microbial selective element enrichments and mobilizations, so it is recommended to include interpretations based on mineralogy and microtextures to determine consistency with these proxies (Bíró et al., 2015).

Microtextural observation show that partly pyritized Fe-rich biomats in the Úrkút black shale characterize the entire sections. This observation also applies to the Mn ore. Fe-rich biomats form under suboxic (Eh: +0.3 V) neutrophylic conditions (Fig. 5), which fits well with conclusions from Fortin et al. (1997), Konhauser (1998), and Konhauser et al. (2012). The Úrkút black shale is fine gained, and silty terrestrial debris does not occur, consistent with our interpretation of the microtextures.

5.2. Mineralogy of the black shales

Previous studies of the Úrkút Mn-carbonate ore deposit, preliminary investigations of the black shale host rock, together with data presented here provide a comprehensive understanding of the mineralogy. Further, this offers an opportunity for comparisons with other black shales, among them epicontinental shelf black shales of Toarcian age.

The black shale mineral assemblage is similar to that of the ore beds, reflecting similar formation conditions, but the minerals occur in different quantitative amounts that determine whether the rock is ore or waste. The minerals consist of (i) carbonates, like *calcite* (*Mn-calcite*) occurring in the form of biogenic debris of variable size, mainly of plankton and nekton, rarely benthic forms (Polgári et al., 2012a). *Dolomite* grains with a size of tens of µm (often idiomorphic) and showing Mn-metasomatism at the margins of the grains. There are two ideas as the origin of these dolomite grains: (1) windblown particles from sabkha facies (Pekker, 2005); and (2) early diagenetic products of microbially mediated carbonate formation and diagenesis (Dupraz & Viesscher, 2005, Pace et al., 2015; Molnár, 2015 adapted Dupraz and Visscher's model for the Úrkút). *Rhodochrosite* is a very fine-grained microbially mediated early diagenetic mineral, as well as *siderite* (Polgári et al., 1991). Negative δ^{13}C values of carbonate support an organic matter contribution to the mineralization under suboxic conditions in the zone of manganese reduction (Table 3). *Kutnohorite* occurs as vein fillings and impregnations that formed during a later diagenetic stage (Polgári et al., 2007). (ii) *Quartz* has several origins based on textural characteristics, windblown particles, authigenic precipitation, and recrystallized biodebris such as radiolarian tests. Diagenetic segregation of quartz is also noted (Polgári et al. 2012a, 2016; Molnár, 2015). *Goethite* occurs as biomats (Polgári et al. 2012b). (iii) *Clay minerals*, like *smectite* and *celadonite*, are authigenic (Weiszburg et al., 2004ab; Tóth et al. 2010; Polgári et al. 2013a). The clay minerals were proposed to have commonly formed by direct clay precipitation onto microbial cell organic matter and EPS, which resulted in clay-rich primary phases, later accompanied by carbonate precipitation via early diagenesis (Yeshaya & Moshe, 1988; Zavarzin, 2003; stated also for Úrkút by Molnár, 2015). Though the Úrkút black shale-hosted Mn mineralization was mediated by various types of microbial activity (Polgári et al., 2010, 2012ab), it is feasible that the Mn mineralization could have also resulted from high amounts of primary authigenic clay mineralization. In this interpretation, the microbially induced and controlled processes cannot be distinguished. We consider celadonite and smectite as authigenic (Cora, 2009; Tóth et al., 2010; Polgári et al., 2013a), possibly microbially mediated products, while chlorite, kaolinite, and unspecified clay minerals are considered detrital. *Chlorite* and *kaolinite* represent rare terrigenous input (windblown). *K-feldspar* and *plagioclase* originated from volcanic ash falls based on cathodoluminescence evidence (Polgári et al., 2012a). *Zeolite (clinoptilolite*) can result from ash alteration (Polgári, 2001), but has been also shown to fill algal cells (Cora, 2009). (iv) *Pyrite* is a common constituent of early diagenetic processes in the zone of sulfate reduction; (v) *barite* formed as an early diagenetic mineral via plankton decomposition (Polgári et al., 2016). (v) *Gypsum* is the product of alteration of pyrite (Polgári et al. 2012a). (vi) *Apatite* occurs as fish debris, and in some black shale layers its concentration is very high (Polgári et al., 2003b, 2007, 2012a).

The scarce data available on the mineralogy of black shale-hosted Mn indications of the Alpine-Mediterranean region are similar to that characteristic for the Úrkút, like diagenetic rhodochrosite and authigenic smectite and celadonite (Cornelius & Plöchinger, 1952; Gruss, 1956; Polák, 1957; Andrusov, 1965; Germann & Waldvogel, 1971; Germann, 1971; Bernoulli & Jenkyns, 1974; Faupl et al., 1982; Beran et al., 1983; Jenkyns, 1988, Jenkyns et al., 1991; Krainer et al., 1994; Krajewsky et al., 2001; Rantitsch et al., 2003; Jach & Dudek, 2005). In contrast, the mineralogical composition of black shales formed on epicontinental shelves differs from the Úrkút, containing mainly detrital components.

The Toarcian Jet Rock Formation (UK), contains considerable amounts of detrital minerals (Morris, 1980) like muscovite (5-7%), biotite, and chlorite, which are not characteristic for Úrkút, but high amounts of quartz and rare feldspar contents are similar. The high clay mineral content is also similar to Úrkút, but the types of clay minerals are basically different. For example in the Jet Rock, the illite and mixed layer clay minerals represent 55-60%, kaolinite is also high, 35-40%, chlorite is 5%, vermiculite is a trace, and smectite, which is considerable in Úrkút, does not occur in the Jet Rock Formation.

Similarly, the Posidonia Shale of the Dutch Central Graben contains silt-size detrital quartz, dolomite, and kaolinite, rare alkali feldspar, and abundant pyrite, quartz silt, and clay minerals, which constitute most of this and other epicontinental shales (João et al., 2012). The shales contain little carbonate except for authigenic dolomite while in Úrkút contains high amounts of rhodochrosite, which is also characteristic in the black shale. Minor diagenetic dolomite occurs in the Úrkút black shale.

The samples collected from the black shale section of the MRV-ÓSF are predominantly composed of calcite, quartz, kaolinite, illite±muscovite, and bituminite material (Raucsik & Varga, 2008b). Additionally, pyrite, illite/smectite mixed-layer minerals, chlorite, rare plagioclase and K-feldspar are also present. Moreover, there are some secondary minerals such as goethite and gypsum, reflecting outcrop weathering. The clay fraction of the MRV-ÓSF black shale samples is dominated by kaolinite (Raucsik & Varga, 2008a) 50–80%, average 67.5% and illite (15–50%, average 30%); random I/S mixed-layer minerals occur in small quantities (from trace amounts to 5–10%), in places with traces of chlorite. Hence, in contrast to the Úrkút, the MRV-ÓSF black shale contains mainly detrital components. Based on clay mineralogy, Raucsik and Merényi (2000) inferred the connection between an upwelling system and climate change (more humid) of the provenance area, which does not apply to the Úrkút because of the predominance of authigenic minerals.

Dera et al. (2009) assessed the Europe-wide distribution of clay minerals deposited through the late Pliensbachian and early Toarcian and recognised that significant kaolinite enrichment occurred within the *falciferum* Zone, broadly coeval with the $\delta^{13}C$ excursion on epicontinental shelf areas. This relative increase in kaolinite abundance was interpreted as evidence for highly efficient continental runoff under a warm, humid climate, which did not reach the Úrkút basin.

5.3. Calculation of environmental conditions based on mineral composition

Both the black shale and the ore are composed mainly of authigenic minerals together with calcite biodebris, ash, and other windblown particles (Table 2). Some authigenic and terrigenous detrital minerals were preserved while others were transformed to other minerals during diagenesis. Formation of various authigenic and diagenetic minerals occurred through both microbially mediated processes and through inorganic processes. A starved basin with variable but dominant authigenic mineralization was determined by quantification of mineral assemblages. The authigenic mineral content exceeds the terrigenous (allothigenic) content in all the black shale beds; in Bs1 this ratio is ~90:10, and is also high in Bs2 (~60-40), and Bs3-4 (~70-30) (Table 2; Figs. 7a, 8a). Based on different distributions of the minerals, the environmental conditions during black shale formation can be inferred (Table 5). The ore-forming stages are summarized on Fig. 7b, 8b, which indicate that the processes of ore formation started at a very early stage and represent important contributions in all the black shale beds. The ore-forming processes were strongest in Bs1, where as much as 85% of the black shale is composed of authigenic minerals related to ore formation, though the data show high variability, down to 15%. The ore-forming processes decreased in Bs2 (17%) and increased again in Bs3-4 (35-40%). This does not mean that all the authigenic minerals formed are ore minerals. Along with the authigenic ore-forming minerals, background sedimentation of the black shale continued (Fig. 8c) and the whole system was affected by diagenesis (Fig. 8d). Microbially mediated chemical reactions were involved in the formation of all the black shale beds, such as contributions of authigenic biogenic minerals from 60-90% including pyrite, or 45-90% without pyrite (Fig. 7c, 8e1-2). Ash sedimentation also comprises up to 30% of some beds (Fig. 8f). Distribution of windblown detritus is considerable in some beds (up to 30%) (Fig. 8g). Biodetritus represented by calcite tests was a basic constituent comprising up to more than 40% of some beds (Fig. 8h).

The black shale basin was a structurally controlled starved depocentre because deep ocean between the continent and the Úrkút basin blocked most terrestrial input. The main mass of sediment that comprises the black shale is authigenic clay and ore minerals that originated most probably from geothermally generated hydrothermal fluids, which has also been proposed as the source of the metals (Polgári et al., 2012a). These processes took place from the beginning of the change from limestone/marlstone deposition to deposition of Bs1, but the ore did not form immediately, probably because the oxygen supply for enzymatic Mn(II) oxidation was insufficient. However, Mn carbonate-rich laminae did form in the Bs1 very close to its contact with the underlying carbonate. The sharp contact between the limestone/marlstone footwall and the ore deposit, initiated during formation of Bs1, could have resulted from the enzymatic oxidation of a huge amount of Mn and Fe. This was a process that reduced pH that blocked carbonate formation, which is consistent with the research of Ehrlich (2015). At the same time, the venting fluids produced authigenic clay minerals directly on organic matter and EPS as described by Yeshaya & Moshe (1988) and Zavarzin (2003). The accumulation of microbially produced highly reactive organic matter resulted in mass-balance change after burial and, during early diagenesis; the sediment became anoxic in the zone of sulfate reduction where pyrite formed. A major part of the organic matter is found in a highly decomposed form of bituminite and lamalginite in the section, while the ratio of the more resistant macerals to microbial attack like vitrinite, inertinite and telalginites relatively increased. Other minerals like barite and zeolite also formed during early diagenesis. Paleoproxy calculations indicate similar conditions existed during accumulation of the black shale and the ore (Table 3).

A distal hydrothermally and microbially induced clay mineral-rich authigenic assemblage (marlstone) is an accurate description of the black shale, in which distinct Mn-carbonate ore beds (Mn-rich laminae) formed from close to the very beginning, when the oxygen supply in the sedimentary basin was high enough for enzymatic Mn(II) oxidation (enzymatic Mn(II) oxidation engine)(Fig. 9). Changes of hydrothermal activity cannot be excluded as a mechanism for initiation of ore deposition.

Our results concerning oxygen supply are different than that of the Jet Rock Formation, which accumulated in poorly oxygenated bottom waters, and consequently has high organic carbon contents, 11.8% (max: 35%; Morris, 1980), which is much higher than that in Úrkút. The Posidonia Shale shows that organic matter accumulation and preservation, high bioproductivity, continuous or periodic anoxia, and high sedimentation rates were closely connected with paleoenvironmental changes in the shallow-water sedimentary basin (Röhl et al., 2001; Schmid-Röhl et al., 2002; João et al., 2012). Kemp and Izumi (2014) reported similar conditions (shallow-water, fluvial course-grained terrestrial debris contributions) for a section deposited on the northwestern margin of Panthalassa and now exposed in southwest Japan. These examples contrast with the Úrkút basin, which was deeper water, under storm wave base.

According Raucsik and Varga (2008b) and based on Jenkyns (1985), the MRV-ÓSF Bs formed under intense upwelling and high plankton productivity, which caused the accumulation of large amounts of organic matter in the epicontinental sea on the European shelf. Though the upwelling and moderate to high productivity was determined for the Úrkút Basin, and also a similarity in marine algae origin of the organic matter exists, the Úrkút shale accumulated under a different geodynamic regime, a pelagic marine environment along a rifting continental margin, which fits well with comparable scenarios described by Bernoulli and Jenkyns (1974), Jenkyns et al. (1991), Channel et al. (1992), and others.

5.5. Organic geochemistry

Vető et al. (1995) determined a predominantly marine algal origin for the organic matter, which fits well with our data for the Bs2 section. However, different features of Bs2 compared to Bs1 and Bs3-4 indicate a change in OM deposition although differences are too small to be interpreted on the basis of our preliminary data. Present results show a quasi-uniform, mixed terrestrial and marine origin of immature OM in all the Bs beds, with additional contributions of algae or bacteria to the Bs2 OM complement. Possible trends in Bs2 suggest that study of the central parts of Bs2 would be fruitful, but sampling would require a tunnel driven in the mine.

Major components of maceral composition along the whole Úrkút section (including the ores) are liptinites (bituminite and liptodetrinite), with a 10-12% contribution of laminated alginite. Vitrinite and inertinite also occur, but only as minor components. Intense biodegradation of trace fossils and relative increase of morphologically recognisable liptinites (Tasmanites-type solitary alga) can be observed in the ore, due to the in situ oxidation and consumption of less resistant bituminite, laminated alginate, and liptodetrinite of planktonic origin (Hámor-Vidó, 2015). A less intense decomposition of bituminite and laminated alginite (together with the transformation of pyrite to iron oxyhydroxides), as described in the MRV-ÓSF, is interpreted as a late-stage oxidation of the section by Varga et al. (2007). They stated that the maceral composition of the black shale and the underlying calcareous marl are similar to the Úrkút black shales: liptinite (bituminite, alginate, liptodetrinite) is dominant (above 95%), and the organic-matter content is higher in the black shales than in the marlstone. For both in Úrkút and MRV-ÓSF, the bituminite content is highest in the black shales with flaser texture (Varga et al., 2007; Hámor-Vidó, 2015).

The medium to low HI values of the immature OM (Polgári et al., 1992) reflect oxidative loss of hydrogen-rich marine OM during diagenesis, thus precursor OM is assumed to be type II kerogen through the whole section (Fig. 10). Maceral composition and GC traces of non-aromatic hydrocarbons show limited terrestrial contributions, which corroborates this assumption.

Comparing our data with those of Hollander et al. (1991), Katz (1994), Sælen et al. (2000), Röhl et al. (2001), Schmid-Röhl et al. (2002), Deconinck et al. (2003), and Varga et al. (2007), we can see significant differences between the sample sets studied (Fig. 11). Bs1 and Bs3-4 are characterised by low TOC, S2, and HI compared to black shales of the MRV-ÓSF (Varga et al., 2007). T_{max} values are in the same range (<430°C) reflecting immaturity of OM in both sample sets. Unlike the MRV-ÓSF black shale, only some of Bs2 samples reach the range of fair or better source-rock potential. We have to note that the MRV-ÓSF black shale rocks are considered to be weathered, which caused the measured S2 and HI to be lower than the original (Hollander et al., 1991; Katz, 1994; Sælen et al., 2000; Röhl et al., 2001; Schmid-Röhl et al., 2002; Deconinck et al., 2003; Varga et al., 2007).

Figures 12a, b show comparisons of our samples with significant Toarcian black shales (Posidonia Shale, Jet Rock, and Schistes Carton of the Paris Basin) based on carbon isotopic compositions of organic matter, TOC, and HI. No obvious differences occur but HI and TOC values are smaller in Bs samples, except for two Bs2 samples, and the $\delta^{13}C_{Corg}$ (VPDB) values of Bs1 and Bs2 differ from those of comparable Toarcian shales, except for some Posidonian Shale samples. Bs3-4 samples differ partially as well but with more overlap (Hollander et al., 1991; Katz, 1994; Sælen et al., 2000; Schmid-Röhl, 1999, 2002; Röhl et al., 2001; Schmid-Röhl et al., Deconinck et al., 2003; Varga et al., 2007).

The isotopic composition of carbonate in the Úrkút black shale also differs from that of MRV-ÓSF Bs (Fig. 13). Here, we observed that oxygen isotopic compositions vary by about -2‰ (–5‰ to –2‰ SMOW), and $\delta^{13}C$ values range from –2‰ to –12‰ (VPDB), with one exceptionally negative Bs2 sample. Varga et al. (2007) concluded that the isotopic compositions of carbonate from MRV-ÓSF Bs, $\delta^{13}C$ –6‰ to 0‰ (VPDB) and $\delta^{18}O$ –4‰ to –13 ‰ (SMOW), reflect a high water-to-rock ratio and homogenous late-stage diagenetic fluids. Thus, these isotopic values cannot be used to assess temperature and salinity of the depositional basin or early diagenetic environment.

High values of TOC and HI are found more than a meter above the main ore bed-Bs2 boundary up to the base of second ore bed, i.e. the inner parts of Bs2 contain better preserved OM. A weak correlation exists between carbonate content and carbon isotopic composition. The increase of carbonate generation is connected to the bacterial decomposition of reactive algal OM, and isotopically light carbon is incorporated into the carbonate formed. We can assume that the variation of the data is probably due to the periods of ore formation, which are governed by changes in the redox conditions at the sediment-water interface. The pristane to phytane ratio (Pr/Ph) in the black shales falls between 0.77 - 1.01 suggesting also an anoxic-dysoxic diagenetic environment (Polgári et al., 2000). However, non-bacterial carbonate formation cannot be excluded, especially in the Bs3-4 section.

We cannot exclude that the OM of MRV-ÓSF black shale and Úrkút black shales originated from similar precursor organic matter, with differences in paleogeography (e.g. decrease of salinity in MRV-ÓSF Bs), and a major difference being ore mineralization, which did not take place in the MRV-ÓSF Bs. However, the differences in the geochemistry of OM do not by all means reflect distinct depositional environments and perhaps result from the partial oxidation and biodegradation (bacterial consumption of) H-rich OM to form Mn and Fe-carbonates, and some pyrite , and they reflect the low preservation of primary liptinites and the elevation of decomposed constituents of fluorescing and non-fluorescing bituminites.

We note that the presence of a carbon isotopic excursion (CIE) representative of the Toarcian Oceanic Anoxic Event (T-OAE) cannot be verified in the Úrkút section even though Úrkút deposition occurred during that time interval (*falciferum* Zone). Two plausible explanations are offered: Polgári et al. (2012b) suggested an extremely fast (several hundred years) process of ore formation and sedimentation in the main ore bed, so that the whole process may have taken place over a small time interval during the T-OAE. This would explain the relatively negative $\delta^{13}C_{PDBCorg}$ values. Hence, the onset and endpoint of the CIE may not have been recorded at Úrkút. On the other hand, the intense diagenetic alteration of OM (decomposition and formation of carbonaceous ore) may have caused the carbon isotopic composition of residual OM to shift towards less negative values, as was observed by, for example, Vető et al. (1997); note the slight isotopic shift in main ore bed.

6. Conclusions

A mineralogical and geochemical multiple proxy study of the Toarcian black shale that hosts a microbially mediated Mn-carbonate ore deposit at Úrkút in central Hungary was undertaken to determine its petrogenesis and paleoenvironmental setting.

The main conclusions are:

1. The Úrkút black shale is a gray shale, lean in organic matter.

2. The dominant mineralogical assemblage is authigenic rather than detrital.

3. The depocentre was a starved basin during accumulation of the black shale in the sense of diminished input of mineral detritus.

4. The organic matter content and diagenetic anoxic features environment were the result of rapid accumulation of microbial organic matter that resulted from microbial booms accompanied by geothermally generated hydrothermal circulation systems, and the high rate of accumulation of authigenic minerals (clay minerals and proto-ore minerals). The organic matter was trapped and degraded in a suboxic-anoxic diagenetic environment where pyrite was produced, decreasing the abundance of organic matter.

5. The sharp contact between the limestone/marlstone footwall and black shale unit Bs1 and the Mn-ore deposit reflect the initiation of hydrothermal vent systems in the marine basin. The inferred enzymatic Mn and Fe oxidation blocked carbonate formation by decreasing pH.

6. Even though Mn-oxide accumulation started very close to the contact with the underlying unit, accumulation of proto-ore did not initially predominate probably because of oxygen deficiency, because Mn(II) enzymatic oxidation is obligatory to this process. But the system remained suboxic via syngenetic mineral accumulation (Fe-rich biomats), and became anoxic through diagenesis.

7. The separation of black shale beds and ore beds is not distinct throughout the section. Instead, a distal hydrothermally induced clay mineral-rich authigenic assemblage (marlstone) best describes the black shale, in which distinct Mn-oxide proto-ore beds (Mn-rich laminae) formed from nearly the beginning of black shale deposition, when the oxygen supply in the sedimentary basin was insufficient for enzymatic Mn(II) oxidation. Mn-oxide proto-ore

transformed into Mn carbonate ore via microbially mediated processes during early diagenesis. Ore beds resulted where these Mn-rich laminae in the BS were highly enriched and abundant.

8. The drivers of Mn-bearing, relatively low organic matter, marlstone formation, compared to other Torcian black shales, were most probably a combination of regional and local processes. Generation of a tectonic rift system promoted geothermally generated circulation cells and hydrothermal fluids and also initiated microbial blooms. The TR, and other regions of the Tethyan realm supported formation of black shales under this complex set of processes. These black shale-hosted Mn-carbonate deposits are indicators of ancient failed rift systems.

9. The Úrkút black shale and Mn ore paleoenvironmental proxies are very similar. Mineralogy, geochemistry, and organic matter are consistent with previous results of the Úrkút, but differ from those of the Tethyan epicontinental shelf occurrences.

Acknowledgments

The study was supported by Financial Support of Excellence of the Hungarian Academy of Sciences. S. A. Gerdes and N. Zajzon offered samples, which is highly appreciated. We thank the careful reviews and constructive suggestions provided by the anonymous reviewers, and editorial handling.

References

Algeo, T.J., Maynard, J.B. 2004 Trace-element behavior and redox facies in core shales of Upper Pennsylvanian Kansas-type cyclothems. Chemical Geology, 206/3–4, 289–318.

Andrusov, D. 1965 Geologie der Tschechoslowakischen Karpaten, II. Akad.-Verlag, Berlin. 443 pp.

Bárdossy G., Bottyán, L., Gadó, P., Griger, Á., Sasvári, J. 1980 Autmated quantitave phase analysis of bauxites, *American Mineralogist*, **65**, 135-141

Bargar, J.R., Tebo, B.M., Bergmann, U., Webb, S.M., Glatzel, P., Chiu, V.Q., Villalobos, M. 2005. Biotic and abiotic products ofMn(II) oxidation by spores of the marine Bacillus sp. strain SG-1. Am. Mineral. 90, 143–154.

Bassoullet, J.E., Elmi, S., Poisson, A., Cecca, E., Bellion, Y., Guiraud, R., Baudin, E. 1993 Mid Toarcian. - In: Dercourt, J., Ricou, L.E., Vrielynck, B. (Eds) Atlas Tethys Paleoenvironmental Maps. BEICIP-FRANLAB, Rueil-Malmaison

Bau M., Dulski P. 1996 Distribution of yttrium and rare-earth elements in the Penge and Kuruman iron-formations, Transvaal Suergroup, South Africa. *Precambrian Research*, **79/1–2**, 37–55.

Bau M., Koschnisky A., Dulski P., Hein J. 1996 Comparison of the partitioning behaviours of yttrium, rare earth elements, and titanium between hydrogenetic marine ferromanganese crusts and seawater. *Geochimica et Cosmochimica Acta*, **60/10**, 1709–1725.

Beran, A., Faupl, P., Hamilton, W. 1983 Die Manganschiefer der Strubbergschichten (Nördliche Kalkalpen, Österreich — eine diagenetisch gepragte Mangankarbonatvererzung. TMPM Tscgermaks Min Petr Mitt, 31, pp. 175–192.

Bernoulli, D., Jenkyns, H.C. 1974 Alpine, Mediterranean and Central Atlantic Mesozoic facies in relation to the early evolution of the Tethys. In: Dott, R.H., Shaver, R.H. (Eds.), Modern and Ancient Geosynclinal Sedimentation: SEPM Spec. Publ., 19, pp. 129–187.

Bíró, L., Polgári, M., M. Tóth, T., Vígh, T., Kávási, N., Sahoo, S.K. 2015 Terrestrial radioisotopes as paleoenvironmental proxies in sedimentary formations. Journal of Radioanalytical and Nuclear Chemistry, 306:(1) pp. 289-293.

Bolhar R., Kamber BS., Moorbath S., Fedo CM., Whitehouse MJ. 2004 Characterisation of early Archaean chemical sediments by trace element signatures. *Earth Planetary Science Letters*, **222**, 43–60.

Bright C.A., Cruse AM., Lyons TW., MacLeod KG., Glascock MD., Ethington RL. 2009 Seawater rare-eart element patterns preserved in apatite of Pennsylvanian conodonts? *Geochimica et Cosmochimica Acta*, **73,** 1609–1624.

Brumsack H-J. 2006 The trace metal content of recent organic carbon-rich sediments: implications for Cretaceous black shale formation. *Palaeogeography, Palaeoclimatology, Palaeoecology*, **232**, 344–361.

Campbell, F.A. and Williams, G.D. 1965 Chemical composition of shales of Mannville Group (Lower Cretaceous) of Central Alberta, Canada. AAPG Bull., 49/1, 81-87.

Channell, J. E. T., Brandner, R., Spieler A., Stoner, J. S. 1992 Paleomagnetism and paleogeography of the Northern Calcareous Alps (Austria). Tectonics, 11/4: 792-810.

Cora, I. 2009. Mineralogical Study of the Úrkút Mn Carbonate Ore. Thesis, Eötvös University, Budapest, 120 p.

Cornelius, H.P., Plöchinger, B. 1952 Der Tennengebirgs-N-Rand mit seinen Manganerzen und die Berge im Bereich des Lammertales. Jb. Geol. B-A 10–225.

Cseh Németh, J., Grasselly, Gy., Szabó, Z. 1980 Sedimentary manganese deposits of Hungary. In: Varentsov, I.M., Grasselly, Gy. (eds), Geology and Geochemistry of Manganese. Akadémiai Kiadó (Budapest) Vol. 2, 199-221.

Csontos, L., Vörös, A. 2004 Mesozoic plate tectonic reconstruction of the Carpathian region. Palaeogeography, Palaeoclimatology, Palaeoecology, 210, 1-56.

Deconinck, J.-F., Hesselbo, S.P., Debuisser, N., Averbuch, O., Baudin, E., Bessa, J. 2003 Environmental controls on clay mineralogy of an Early Jurassic mudrock (Blue Lias Formation, southern England). International Journal of Earth Sciences 92, 255-266.

Dera, G., Pellenard, P., Niege, P., Deconinck, J.-F., Puceat, E., Dommergues, J.-L. 2009 Distribution of clay minerals in Early Jurassic peritethyan seas: palaeoclimatic significance inferred from multiproxy comparisions. Palaeogeography, Palaeoclimatology, Palaeoecology 271, 39–51.

Duarte, L.V. 1998 Clay minerals and geochemical evolution in the Toarcian–lower Aalenian of the Lusitanian basin (Portugal). — Cuadernos de Geología Ibérica 24, 69–98.

Dulai, A., Suba, Zs., Szarka, A. 1992 Toarci (alsójura) szervesanyagdús fekete pala a mecseki Rékavölgyben. Földtani Közlöny 122, 1, 67-87.

DUPRAZ, C., VIESSCHER, P. T. 2003 Microbial lithification in marine stromatolites and hypersaline mats, *Trends in Micobiology*, **13**, 429-438.

Dypvik, H., Hams, N.B. 2001 Geochemical facies analysis of fine-grained siliciclastics using Th/U, Zr/Rb and (Zr+Rb) /Sr ratios. Chem. Geol., 181, 131-146.

Ehrlich, H. L. 2015 *Geomicorbiology* (6th edition). Marcell Dekker Inc., 635 pp.

Espitalié, J., Deroo, G., Marquis, F. 1985 Rock Eval pyrolysis and its applications. Revue de l'Institut Francais du Pétrole Part I 40, 653–578, Part II 40, 755– 784, Part III 41, 73– 89.

Farrimond, P., Eglinton, G., Brassell, C., Jenkyns,H.C. 1989 Toarcian anoxic event in Europe: an organic geochemical study. Mar. Pet. Geol. 6, 136–147.

Faupl, P., Beran, A., Hamilton, W. 1982 Erkundung auf Mangan in den Strubbergschichten im Gebiet Golling-Abtenau (Salzburg). Ein Kurzbericht über das Projekt SA 14. Arch. Lagerstforsch. Geol. B-A 2, 171.

Figueiredo, M.M., Martins, A.G., Gamelas, J.A.F. 2012 Characterization of bone and bone-based graft materials using FTIR spectroscopy. In: Theophanides Theophile (Ed.) Infrared Spectroscopy - Life and Biomedical Sciences. InTech. DOI: 10.5772/36379.

Fortin, D., Ferris, F.G., and Beveridge, T.J. 1997 Surface-mediated mineral development by bacteria, *in* Banfield, J., and Nealson, K.H., eds., Geomicrobiology: Interactions between microbes and minerals: Mineralogical Society of America Reviews in Mineralogy Volume 35, p. 162–180.

Géczy, B. 1973 The Lower Jurassic ammonite faunas of the Southern Bakony (Transdanubia, Hungary). Ann. Univ. Sci. Bp. Sect. Geol. 17, 181–190.

Germann, K. 1971 Mangan-Eisen-führende Knollen und Krusten in jurassischen Rotkalken der Nördlichen Kalkalpen. N. Jb. Geol. Paläont. Mh. 3, 133–156.

Germann, K., Waldvogel, F. 1971 Mineralparagenesen und Metallgehalte der “Manganschiefer” (unteres Toarcian) in den Allgau-Schichten der Allgauer und Lechtaler Alpen. N. Jb. Geol. Palaeont. Abh. 139, 316–345.

Glotch, T.D., Rossman, G.R. 2009 Mid-infrared reflectance spectra and optical constants of six iron oxide/oxyhydroxide phases. Icarus 204, 663–671.

Gruss, H. 1956 Exhalativ-sedimentare Mangankarbonatlagerstatten mit besonderer Berücksichtingung der liassichen Vorkommen in den Berchtesgadener und Salzburger Alpen. N. Jhb. Min. Abh. 92, 47–107

Haas, J. 1994 Mesozoic. University Book. Eötvös Publishing House, Budapest. 119 pp.

Haas, J. 2012 Influence of global, regional, and local factors on the genesis of the Jurassic manganese ore formation in the Transdanubian Range, Hungary. Ore Geol. Rev. 47, 77–86

Hallam, A. 1967 Sedimentology and palaeogeographic significance of certain red limestones and associated beds in the Lias of the Alpine region. Soc. J. Geol. 3, 195–220.

Hallam, A. 1981 A revised sea-level curve for the early Jurassic. Geological Society of London, Journal, 138, 735-743.

Hámor-Vidó, M. 2015 Observation of early diagenetic processes through organic matter changes in the Toarcian Úrkút Manganese Formation in Hungary. 2015 ICCP Symposium on "Coal and Organic Petrology – In: J. Kus, P. David, S. Kalaitzidis, H-M. Schulz & R.F. Sachsenhofer (Eds.). ICCP Program & Abstract Book. 67th Annual Meeting of the International Committee for Coal and Organic Petrology, September 5-11. 2015 Potsdam, Germany. Schriftenreihe der Deutschen Gesellschaft für Geowissenschaften Heft 87, 88.

Hesselbo, S.P., Gröcke, D.R., Jenkyns, H.C., Bjerrum, C.J., Farrimond, E., Morgans Bell, H.S., Green, O.R. 2000 Massive dissociation of gas hydrate during a Jurassic oceanic anoxic event. Nature 406, 392-395.

Hollander, D.J., Bessereau, G., Belin, S., Hue, A.Y., Houzay, J.P. 1991 Organic matter in the early Toarcian shales, Paris Basin, France: A response to environmental changes. Revue de l'Institut Français du Pétrole 46/5, 543-562.

Jach, R., Dudek, T. 2005 Origin of a Toarcian manganese carbonate/silicate deposit from the Krížna unit, Tatra Mountains, Poland. Chem. Geol. 224, 136–152.

Jenkyns, H.C. 1985 The early Toarcian and Cenomanian-Turonian anoxic events in Europe: comparisons and contrasts. Geologische Rundschau 74, 3, 505-518.

Jenkyns, H.C. 1988 The early Toarcian (Jurassic) anoxic event: stratigraphy, sedimentary, and geochemical evidence. American Journal of Science 288, 101-151.

Jenkyns, H.C. 2010 Geochemistry of oceanic anoxic events. Geochemistry, Geophysics, Geosystems 11, 3, 1-30.

Jenkyns, H.C., Clayton, C.J. 1997 Lower Jurassic epicontinental carbonates and mudstones from England and Wales: Chemostratigraphic signals and the early Toarcian anoxic event. Sedimentology 44, 687-706.

Jenkyns, H.C., Géczy, B., Marshall, J.D. 1991 Manganese deposits of central Europe and the Early Toarcian anoxic event. J. Geol. 99, 137–150.

Jenkyns, H.C., Gröcke, D.R., Hesselbo, S.E. 2001 Nitrogen isotope evidence for water mass denitrification during the early Toarcian (Jurassic) anoxic event. Palaeoceanography 16, 593-603.

João, T-A., Dirkx, R., Veld, H., Klaver, G., De Boer, P.L. 2012 Toarcian black shales in the Dutch Central Graben: Record of energetic, variable depositional conditions during an Oceanic Anoxic Event. Journal of Sedimentary Research, 82, 104-120. DOI: 10.2110/jsr.2012.5

Katz, B.J. 1994 The Schistes Carton – the Lower Toarcian of the Paris Basin. In: Katz, B.J. (Ed.) Petroleum Source Rocks. Springer-Verlag, Berlin-Heidelberg-New York, 51-65.

Kázmér, M. & Kovács S. 1985 Permian-Paleogene paleogeography along the eastern part of the Insubric-Periadriatic lineament system: Evidence for continental escape of the Bakony-Drauzug unit, *Acta Geologica Hungarica*, **28**, 71–84.

Kearey, P. 2001 The New Penguin Dictionary of Geology, Penguin, London, p. 30.

Kemp, D. B. , Coe, A. L., Cohen, A. S. & Schwark, L. 2005 Astronomical pacing of methane release in the Early Jurassic period. — Nature 423 , 396-399.

Kemp, D.B., Kentaro Izumi, K. 2014 Multiproxy geochemical analysis of a Panthalassic margin record of the early Toarcian oceanic anoxic event (Toyora area, Japan). Palaeogeography, Palaeoclimatology, Palaeoecology 414, 332–341.

Konhauser, K. (Ed.) 2012 Fundamentals of Geomicrobiology, Wiley - Blackwell Science Ltd, 50-210.

Konhauser, K. 1998 Diversity of bacterial iron mineralization, *Earth-Science Review*, 43, 91–121.

Krainer, K., Mostler, H., Haditsch, J.G. 1994 Jurassische Beckenbildung in den Nördlichen Kalkalpen bei Lofer (Salzburg) unter besonderer Berücksichtigung der Manganerz-Genese. Abh. Geol. B-A 50, 257–293.

Krajewsky, K.P., Lefeld, J., Lacka, B. 2001 Early diagenetic processes in the formation of carbonate-hosted Mn ore deposit (Lower Jurassic, Tatra Mountains) as indicated from its carbon isotopic record. Bull. Pol. Acad. Sci. 49 (1), 13–29.

Küspert, W. 1982 Environmental changes during oil shale deposition as deduced from stable isotope ratios. — In: EINSALE, G. & SEILACHER, A. (Eds): Cyclic and Event Stratification, Springer-Verlag, New York, 482-501.

Madejová, J., Komadel, P. 2001 Baseline studies of the clay minerals society source clays: infrared methods. Clays and Clay Minerals 49, 410-432.

McArthur, J., Algeo, T., van de Schottbrugge, B., Li, Q., Howarth, R. 2008 Basinal restriction, black shales, Re-Os dating, and the Early Toarcian (Jurassic) oceanic anoxic event. Paleoceanography, 23, 1-22. PA4217, DOI 10.1029/2008PA001607.

Milota, K. 1992 Geochemistry and interpretation of hydrocarbons of Mesozoic formations of Mecsek-Nagykőrös-Debrecen zone according to aspects of raw material exploration. Thesis, University of Szeged, 96 p.

Molnár, Zs. 2015 Initial Fe-Mn-oxide ore indications in the footwall of the Toarcian Úrkút Mn-carbonate ore deposit, Hungary. Thesis. Eötvös University, Budapest, 208 p.

Morris, K.A. 1980 Comparison of major sequences of organic-rich mud deposition in the British Jurassic. Geological Society of London, Journal, 137, 157-170.

Müller, C. M., Pejcic, B., Esteban, L., Delle Piane, C., Raven, M., Mizaikoff, B. 2014 Infrared Attenuated Total Reflectance Spectroscopy: An Innovative Strategy for Analyzing Mineral Components in Energy Relevant Systems. Scientific Reports 4, Article number: 6764. DOI: 10.1038/srep06764.

Nesbitt, H.W. and Young, G.M. 1982 Early Proterozoic climates and plate motions inferred from major element chemistry of lutites. Nature, 199, 715-717.

Neuendorf, K.K.E., Mehl, J.P.Jr., Jackson, J.A. (Eds.) 2005 Glossary of , 5th ed. Am. Geol. Inst., Alexandria, Va, p. 72.

Nothdruft LD., Gregory EW., Balz SK. 2004 Rare earth element geochemistry of Late Devonian reefal carbonates, Canning Basin, Western Australia: Confirmation of a seawater RFF proxy in ancient limestones. *Geochimica et Cosmochimica Acta*, **68/2**, 263–283.

Pace, A., Bouton, A., Bourillot, R., Vennin, E., Visscher, P., Dupraz, C., Thomazo, C., Galaup. S., Kwasniewski, A. 2015 Microbial and Physicochemical Steps Leading to the Mineralization of the Great Salt Lake Microbialites (*Goldschmidt conference, 2015 absztrakt, 2374*).

Pálfy, J., Smith, E.L. 2000 Synchrony between Early Jurassic extinction, oceanic anoxic event, and the Karoo-Ferrar flood basalt volcanism. Geology 28/8, 747-750.

Pálfy, J., Smith, E.L., Mortensen, J.K. 2002 Dating the end-Triassic and Early Jurassic mass extinctions, correlative large igneous provinces, and isotopic events. In: Koeberl, C., Macleod, K.G. (Eds) Catastrophic Events & Mass Extinctions. Impacts and Beyond. Geological Society of America, Special Papers 356, 523-532.

Parikh, S. J., Chorover, J. 2006 ATR-FTIR spectroscopy reveals bond formation during bacterial adhesion to iron oxide. Langmuir 22, 20, 8492-8500.

Pekker, P. 2005 Mineralogy of the Eplény Limestone Formation, Úrkút, Hungary Thesis, Eötvös University, Budapest, 3-55.

Polák, S. 1957 Manganese ores of the Malé Karpaty Mts. Geol. práce Zos. 47, 39–83.

Polgári, M. 1993 Manganese geochemistry reflected by black shale formation and diagenetic processes — model of formation of the carbonatic manganese ore of Úrkút. Special Series of Hungarian Geological Institute. Karpati Publish House, Ushgorod. 211 pp.

Polgári, M. 2001 Contribution of volcanic material? – A new aspect oft he genesis oft he black shale-hosted Jurassic Mn-carbonate ore formation, Úrkút Basin, Hungary. Acta Geologica Hungarica, 44/4, 419-438.

Polgari, M., Bajnóczi, B., Kis, V.K., Gotze, J., Dobosi, G., Tóth, M., Vígh, T. 2007 Mineralogical and cathodoluminescence characteristics of Ca-rich kutnohorite from the Úrkút Mn-carbonate mineralization, Hungary. Mineralogical Magazine 71, 5, 493-508.

Polgári, M., Bíró, L., Pál-Molnár, E., Dobosi, G., Bajnóczi, B., Németh, T., Kovács Kis, V., Vígh, T. 2013b Rhodochrosite-bearing concretions from a Jurassic Manganese ore mineralization, Úrkút, Hungary. Carpathian Journal of Earth and Environmental Sciences 8, 4, 139-146.

Polgári, M., Dobosi, G., Horváth, P., Rálischné Felgenhauer, E., Vigh, T. 2003a As-bearing pyrite at Úrkút and in the Jurassic layers of borehole Iharosberény-I. Bull. Hung. Geol. Surv. 133 (4), 69–475 (in Hungarian with English abstract).

Polgári, M., Hein, J.R., Németh, T., Pál-Molnár, E., Vígh, T. 2013a Celadonite and smectite formation in the Úrkút Mn-carbonate ore deposit (Hungary). Sedimentary Geology 294, 157-163.

Polgári, M., Hein, J.R., Tóth, A.L., Pál-Molnár, E., Vígh, T., Bíró, L., Fintor, K. 2012b Microbial action formed Jurassic Mn-carbonate ore deposit in only a few hundred years (Úrkút, Hungary). Geology 40, 10, 903-906.

Polgári, M., Hein, J.R., Tóth, M., Brukner-Wein, A., Vígh, T., Bíró, L., Cserháti, C. 2010 Genesis of a regionally widespread celadonitic chert ironstone bed overlying upper Lias manganese deposits, Hungary. Journal of the Geological Society 167, 2, 313-328.

Polgári, M., Hein, J.R., Vígh, T., Szabó-Drubina, M., Fórizs, I., Bíró, L., Müller, A., Tóth, L. 2012a Microbial processes and the origin of the Úrkút manganese deposit, Hungary. Ore Geology Reviews 47, 87-109.

Polgári, M., Molák, B., Surova, É. 1992 An organic geochemical study to compare Jurassic black shale-hosted manganese carbonate deposits: Úrkút, Hungary, and Branisko Mountains, East Slovakia. Exploration and Mining Geology 1, 1, 63-67.

Polgári, M., Németh, T., Pál-Molnár, E., Futó, I., Vígh, T., Mojzsis, J.S. 2016 Correlated chemostratigraphy of Mn-carbonate microbialites (Úrkút, Hungary). Gondwana Research 29, 1, 278-289.

Polgári, M., Okita, P.M., Hein, J.R. 1991 Stable isotope evidence for the origin of the Úrkút manganese ore deposit, Hungary. Journal of Sedimentary Petrology 61, 3, 384-393.

Polgári, M., Szabó, Z., Szabó-Drubina, M., Hein, R.J., Yeh, H.W. 2005 A porous silica rock ("Tripoli") in the footwall of the Jurassic Úrkút manganese deposit, Hungary: composition, and origin through carbonate dissolution. Sedimentary Geology 177, 1-2, 87-96.

Polgári, M., Szabó, Z., Szederkényi, T. (Eds.) 2000 Manganese Ores in Hungary – In Commemoration of Professor Gyula Grasselly – Hungarian Academy of Sciences. Juhász Publishing House, Szeged. 675 pp.

Polgári, M., Szabó-Drubina, M., Hein, J.R. 2003b Phosphogenesis in Jurassic black shale-hosted Mn-carbonate deposits, Úrkút and Eplény, Hungary: Investigations on archive sample drillcore Úrkút-136. Bull. Hung. Geol. Surv. 133 (1), 37–48.

Polgári, M., Szabó-Drubina, M., Szabó, Z. 2004 Theoretical model for the Mid-European Jurassic Mn-carbonate mineralization Úrkút, Hungary. Bulletin of Geosciences 79, 1, 53-61.

Rantitsch, G., Melcher, F., Meisel, T., Rainer, T. 2003 Rare earth, major and trace elements in Jurassic manganese shales of the Northern Calcareous Alps: hydrothermal, versus hydrogenous origin of stratiform manganese deposits. Mineral. Pet. 77 (1–2), 109–127.

Raucsik, B., Merényi, L. 2000 Origin and environmental significance of clay minerals in the Lower Jurassic formations of the Mecsek Mts, Hungary. Acta Geologica Hungarica 43/4, 405-429.

Raucsik, B., Varga, A. 2008a Mineralogy of the Lower Toarcian black shale section from the Réka Valley (Óbánya Siltstone Formation, Mecsek Mountains, Hungary): implications for palaeoclimate. Bull. of Hungarian Geological Survey, 138/2, 133–146.

Raucsik, B., Varga, A. 2008b Climato-environmental controls on clay mineralogy of the Hettangial-Bajocian successions of the Mecsek Mountains, Hungary: an evidence for extreme continental weathering during the early Toarcian oceanic anoxic event. Palaeogeography, Palaeoclimatology, Palaeoecology 265, 1, 1-13.

Röhl, H.J., Schmid-Röhl, A., Oschmann, W., Frimmel, A., Schwark, L. 2001 The Posidonia Shale (Lower Toarcian) of SW-Germany: an oxygen-depleted ecosystem controlled by sea level and palaeoclimate: Palaeogeography, Palaeoclimatology, Palaeoecology 165, 27–52.

Rosales, I., Quesada, S., Robles, S. 2004 Paleotemperature variations of Early Jurassic seawater recorded in geochemical trends of belemnites from the Basque-Cantabrian basin, northern Spain. Palaeogeography, Palaeoclimatology, Palaeoecology 203, 253-275.

Roy, S. 1981 Manganese Deposits. Academic Press, London. 458 pp.

Sælen, G., Tyson, R.V., Telwes, N., Tabot, M.R. 2000 Contrasting watermass conditions during deposition of the Whitby Mudstone (Lower Jurassic) and Kimmeridge Clay (Upper Jurassic) formations, UK. Palaeogeography, Palaeoclimatology, Palaeoecology 163, 163-196.

Scheffler, K. 2004 Reconstruction of sedimentary environment and climate conditions by multi-geochemical investigations of Late Palaeozoic glacial to postglacial sedimentary sequences from SW-Gondwana. PhD Thesis, Rheinischen Friedrich-Wilhelms-Universität Bonn, Wuppertal, Bonn, Germany, pp. 243.

Schmid-Röhl, A., Röhl, H.J., Oschmann, W., Frimmel, A., Schwark, L. 2002 Paleoenvironmental reconstruction of Lower Toarcian epicontinental black shales (Posidonia Shale, SW Germany): global versus regional control. Geobios 35, 13–20.

Schmitz B., Charisi SD., Thompson EI., Speijer RP. 1996 Barium, SiO_2 (excess), and P_2O_5 as proxies of biological productivity in the Middle East during the Paleocene and the latest Paleocene benthic extinction events. *Terra Nova,* **9/2**, 95–99.

Schwark, L., Frimmel, A. 2004 Chemostratigraphy of the Posidonia Black Shale, SW-Germany: II. Assessment of extent and persistence of photic-zone anoxia using aryl isoprenoid distributions. Chemical Geology 206, 3-4, 231-248.

Song H., Wignall PB., Tong J., Bond DPG., Song H., Lai X., Zhang K., Wang H., Chen Y. 2012 Geochemical evidence from bio-apatite for multiple oceanic anoxic events during

Permian–Triassic transition and the link with end-Permian extinction and recovery. *Earth and Planetary Science Letters*, **353–354**, 12–21.

Szabó, Z., Grasselly, Gy. 1980 Genesis of manganese oxide ore in the Úrkút basin, Hungary. In: Varentsov, I.M., Grasselly, Gy (Eds.), Geology and Geochemistry of Manganese, Vol. 2. Akadémiai Kiadó, Budapest, pp. 223–236.

Szabó-Drubina, M. 1959 Manganese deposits of Hungary. Econ. Geol. 54, 1078–1093.

Taylor, H., Teichmüller, M., Davis, A., Diessel, C.F.K., Littke, R., Robert, P. 1998 Organic Petrology. Borntraeger, Berlin-Stuttgart, 704 pp.

Taylor, S. R., McLenmann S.M. 1995 The geochemical evolution of the continental crust, Rev. Geophys. 33, pp. 241–265.

Tebo, B.M., Bargar, J.R., Clement, B., Dick, G., Murray, K.J., Parker, D., Verity, R., Webb, S. 2004 Manganese biooxide: properties and mechanisms of formation. Ann. Rev. Earth Planet. Sci. 32, 287–328.

Toth JR. 1980 Deposition of submarine crusts rich in manganese and iron. *Geological Society of American Bulletin*, **91**, 44–54.

Tóth, E., Weiszburg, G.T., Jeffries, T., Williams, C.T., Bartha, A., Bertalan, É., Cora, I. 2010 Submicroscopic accessory minerals overprinting clay mineral REE patterns (celadonite–glauconite group examples). Chemical Geology 269, 312–328.

van de Schootbrugge, B., Bailey, T.R., Rosenthal, Y., Falkowski, P.G., Katz, M.E., Wright, J.D., Miller, K.G., Feist-Burkhardt, S. 2005 Early Jurassic climate change and the radiation of organic-walled phytoplankton in the Tethys Ocean. Paleobiol 1–19.

Varga, A., Raucsik, B., Hámor-Vidó, M., Rostási, Á. 2007 Isotope geochemistry and characterization of hydrocarbon potential of black shale from Óbánya Siltstone Formation. Bull. of Hung. Geol. Survey, 137/4, 449-472.

Vető, I. 1993 Quantitative investigation of effect of anaerob bacterial degradation of organic matter of marine sedimentary rocks. Doctor thesis, manuscript. Manuscript Archive, Hungarian Academy of Sciences. D/16.918. 85 pp. (in Hungarian).

Vető, I., Demény, A., Hertelendi, E., Hetényi, M. 1997 Estimation of primary productivity in the Toarcian Tethys — a novel approach based on TOC, reduced sulphur and manganese contents. Palaeogeog. Palaeoclim. Palaeoecol. 132, 355–371.

Vető, I., Hetényi, M., Demény, A., Hertelendi, E. 1995 Hydrogen index as reflecting intensity of sulphidic diagenesis in non-bioturbated shaly sediments. Org. Geochem. 22 (2), 299–310.

Webb, S., Dick, G.J., Bargar, J.R., Tebo, B.M. 2005 Evidence for the presence of Mn (III) intermediates in the bacterial oxidation of Mn(II). Microbiology 102, 5558–5563.

Wedepohl, K.H. 1971 Environmental influences on the chemical composition of shales and clays. In: Ahrens LH., Press F., Runcorn SK., Urey HC. (Eds.) Physics and Chemistry of the Earth, vol. 8. Pergamon, Oxford, 307-331.

Weiszburg, T.G., Nagy, T., Tóth, E., Mizák, J., Varga, Zs, Lovas, GyA, Váczi, T. 2004a A laboratory procedure for separating micas from quartz in clay-sized materials. Acta Mineral. Pet. Szeged 45 (1), 133–139.

Weiszburg, T.G., Tóth, E., Beran, A. 2004b Celadonite, the 10-Å green clay mineral of the manganese carbonate ore, Úrkút, Hungary. Acta Mineralogica et Petrographica 45, 1, 65-80.

Wignall, P.B. 1994 Black Shales. Clarendon Press, Oxford. 124 pp.

Wignall, P.B., Newton, R.J., Little, C.T.S. 2005 The timing of paleoenvironmental change and cause-and-effect relationships during the Early Jurassic mass extinction in Europe : American Journal of Science, 305, 1014-1032.

Yang B., Hu B., Bao Z., Zhang Z. 2011 RFF geochemical characteristics and depositional environment of the black shale-hosted Baiguoyuan Ag-V deposit in Xingshan, Hubei Province, China. *Journal of Rare Earths*, **29/5**, 499–506.

Yeshaya, B.-O., Moshe S. 1988 The role of cell-bound flocculants in coflocculation of benthic cyanobacteria with clay particles. FEMS Microbiology Letters 53, 3–4, 169-174.

Zavarzin, G., A. 2003 Diversity of cianobacterial mats. In: Krumbein W., E. (Ed.) Fossil and Recent Biofilms, **8**, 141-150.

Figure caption

Fig. 1. Palaeogeography of the Early Jurassic of Europe, after Bassoullet et al. (1993), with locations of some lower Toarcian black shale sections (Jenkyns, 1985, 1988; Duarte, 1998).

Fig. 2. Location of study area (a), Tectonic units and main formations of the Úrkút deposit (b), tectonic map of Jurassic Tethyan Realm (c) (modified after Polgári et al., 2012a).

Fig. 3. Profile of black shale host of Mn-carbonate deposit and location of samples; this is a composite log without the ore beds so the thickness of Mn carbonate ore beds and the chert-ironstone are not to scale; the – after cm means below the Mn-carbonate ore beds and the + means above the Mn-carbonate ore beds; Úrkút mine, Shaft No. III, western minefield, +186 mBf); Bs = black shale (Collected by T. Vigh, Mangán Ltd. Úrkút).

Fig. 4. Representative samples. Arrow shows to top of sample according to profile; no arrow: not oriented.

Fig. 5. XRD mineralogy. The two red lines represent ore beds.

Fig. 6. Representative series of photos of partly pyritized Fe-rich biomats, petrographic microscope, transmitted light. (a) Sample FP16A series of Fe-rich biomats (white arrows) and detrital and biogenic debris (black arrows) in fine-grained matrix material (b) Pyritized Fe-rich biomats (p-pyrite); (c) FP22A pyritized Fe-rich biomats (p-pyrite); (d) FP22C Series series of partly pyritized (p) Fe-rich biomats and fish debris (fd, apatite); (e) FP24BB series of partly pyritized (arrows) Fe-rich biomats; (f) Crossed Nicol of (e); (g) Series of partly pyritized Fe-rich biomats (arrows); (h) Series of partly pyritized Fe-rich biomats (arrows) with fish debris (fp) and other detritus. For further details see Fig. 3 and SI 1, 2.

Fig. 7. Box plot diagrams of authigenic and detrital phases (a), components from ore-forming processes (b), and biogenic components (c).

Fig. 8. Contributions from various sources and processes on black shale mineralogy. For details see Table 5. Bold black lines represent ore horizons, bold dashed lines represent hiatus in black shale sections.

Fig. 9. Syngenetic oxygen supply based on mineralogy.

Fig. 10. Total organic carbon (TOC), Hydrogen Index (HI) and kerogen carbon isotope values. (Bs=black shale). Dots: current samples; circles: data from Polgári et al. (1991); squares: data from Vető et al., 1997, triangles: data from Polgári et al. 2000. Vertical axis: distance from the footwall Isztimér Limestone Formation.

Fig. 11. Comparison of kerogen type (a, b) and maturity (b) of Bs1, Bs2 and Bs3-4 with the data from Varga et al. (2007) and other black shale deposits cited therein. The loss of hydrogen-rich algal biomass during diagenesis results in type III kerogen values. Data from Hollander et al. (1991), Katz (1994), Sælen et al. (2000), Röhl et al. (2001), Schmid-Röhl et al. (2002), Deconinck et al. (2003), Varga et al. (2007).

Fig. 12. Carbon isotopic compositions versus TOC (a) and HI (b) values with data from Varga et al. (2007). Dashed lines represent the ranges of data. Significant differences between Úrkút (Bs1, Bs2 and Bs3-4) and other deposits can be seen. *Data from Hollander et al. (1991), Katz (1994), Sælen et al. (2000), Schmid-Röhl (1999, 2002), Röhl et al. (2001), Deconinck et al. (2003), Varga et al. (2007).

Fig. 13. Carbon and oxygen isotopic composition of carbonates; (a) comparison with MRV-ÓSF Bs (*data from Varga et al., 2007). (b) diameter of the dots represents carbonate content (~2–50 wt. %), showing the more negative values of carbonate-rich samples, Úrkút Bs.

Table 1. List of samples

Sample ID	Lithology	Sample ID	Lithology
FP3	Bs2	**1_12**	Bs1
FP4	Bs2	**5_16**	Bs2
FP5	Bs2	**5_17**	Bs2
FP6	Bs2	**5_18**	Bs2
FP7	Bs2	**5_19**	Bs2
FP8	Bs1	**Z/1**	Bs3-4
FP9	Bs2	**Z/2**	Bs3-4
FP10	Bs2	**Z/10'''**	Bs2
FP11	Bs2	**Z/10''**	Bs2
		Z/10'	Bs2
FP15	Bs1	**Z/15**	Bs2
FP16	Bs1		
FP17	Bs1		
FP18	Bs1		
FP19	Bs1		
FP21	Bs3-4		
FP22	Bs3-4		
FP23	Bs2		
FP24,25	Bs2		
1/131025	Bs1		

Table 2. Black shale mineralogy and mineral genesis, grouped by mineral types based on XRD, rock microscopy and IR

Minerals grouped on genetic aspects													
Mineral group	**Minerals**	**Authigenic**		**Biodebris***	**Terrigenous**		**Diagenetic (from authigenic)**		**Authigenic not affected by diagenesis**	**Diagenetic (from terrigenous)**		**Terrigenous not affected by diagenesis**	**Secondary alteration**
		microbially mediated (mm)	non-mm				microbially mediated (mm)	non-mm		microbially mediated (mm)	non-mm		
Carbonates	calcite			*									
	dolomite						*					*	
	rhodochrosite						*						
	kutnohorite							*					
	siderite						*						
Oxides	quartz	*?	*	*	* (wind blown)		*?	*	*			*	
	goethite	*					*						
Phyllosilicates	smectite	*							*				
	celadonite	*							*				
	chlorite, kaolinite (clay)				*							*	
Tectosilicates	K-feldspar				* (volcanic ash)							*	
	plagioclase				* (volcanic ash)							*	
	zeolite (clinoptilolite)										* (tuff alteration, algae-filling)		
Sulfides	pyrite						*	*					
Sulphates	gypsum												*
	barite							*					
Phosphates	apatite			*									

*biodebris is not affected by diagenesis

Table 3. Comparision of chemical paleoenvironmental proxies of the black shale and Mn carbonate ore of Úrkút and Posidonia Shale

Proxy	Black shale (Úrkút)	Mn carbonate ore (Úrkút)	Method	References
A				
Redox	oxic	oxic	U/Th	Yang et al. (2011)
Productivity	Moderate. At one-one sample: footwall, bed No. 2	Important in middle of main ore bed, moderate in bed No. 2	$Y^* = (Y / Al_2O_3)_{minta}$ ´ $(Al_2O_3)_{Upper\ Continental\ Crust}$ Y*: Si, P, Ba	Schmitz et al. (1996)
Enrichment factor (EF median)	Te, **Co**, S, **As**, **Mn**, **Mo**, **Ca** > 5	**Co**, **Mn**, P, **Ca**, **Mo**, Ce, Ga, **As**, Sr > 5	$EF(element) = (element / Al)_{sapmle} / (element / Al)_{Average\ Shale}$	Wedepohl (1971)
	REE 2.3	***REE ~ 4.3***		
	In, Hf, **K**, Ba, **Na** < 1	**K**, Rb, **Na** < 1		
	Max.: Co 15.0; (Te 17.4)	Max.: Co 37.9; Mn 34.6		
Element excess (Xs median)	Te, **Co**, S, **As**, **Mn**, **Mo**, **Ca**, **P**, Ag > 70%	**Co**, **Mn**, **P**, **Ca**, **Mo**, Ce, Ga, **As**, Sr, Fe, Mg, RFF, Ni, Y > 70%	$Ex(element) = element – Al_{sample}$ $(element / Al)_{Average\ Shale}$	Brumsack (2006)
	REE: 56%	***REE: 76%***		
	Na, Ba, K, Hf, In, Rb, Bi < 0%	Na, Rb, K < 0%		
	Max.: Te, Co (93-94%)	Max.: Co, Mn (97%)		
Anomalies				
Pr	0.8	0.8	$Pr/Pr^* = 2\ Pr_{PAAS} / (Ce_{PAAS} + Nd_{PAAS})$	Bau and Dulski (1996)
Ce	1.42 (max. 1.51 main ore bed) cannot accept because of anomaly of Pr	1.35 (max. 2.12 main ore bed) cannot accept because of anomaly of Pr	$Ce_{anom} = Ce_{PAAS} / (2\ Pr_{PAAS} - Nd_{PAAS})$	Bolhar et al. (2004)
La	0.90 cannot accept because of anomaly of Pr	0.88 cannot accept because of anomaly of Pr	$La_{anom} = La_{PAAS} / (3\ Pr_{PAAS} – 2\ Nd_{PAAS})$	Bolhar et al. (2004)
Eu	1.13 (max. 1.21 bed No. 2)	1.08 (max. 1.18 footwall + main ore bed + bed No. 2)	$Eu_{anom} = Eu_{PAAS} / (2/3\ Sm_{PAAS} + 1/3\ Tb_{PAAS})$	Bau and Dulski (1996)
Gd	1.10 normal marine	1.11 normal marine	$Gd_{anom} = Gd_{PAAS} / [(0.33\ Sm_{PAAS}) + (0.67\ Tb_{PAAS})]$	Bau et al. (1996)
Y	0.82 (decreases upward, more intense adsorption)	1.00 (low: footwall, main ore bed + decreases upward in bed No. 2)	$Y_{anom} = 2\ Y_{PAAS} / (Dy_{PAAS} + Ho_{PAAS})$	Bau et al. (1996)
ΔSm_{PAAS}	1.23 (decreases upward: decrease of MREE enrichment)	1.06 (high: footwall, main ore bed + top of bed No. 2)	$\Delta Sm_{PAAS} = Sm - (8\ La_{PAAS} - 5\ Yb_{PAAS}) / 13$	Bright et al. (2009)
(Nd/Yb)$_{PAAS}$ (LRFF/HRFF)	1.11 (decreases upward: decrease of LREE enrichment)	1.27 (decreases upward: decrease of LREE enrichment)		Nothdruft et al. (2004)
(Pr/Sm)$_{PAAS}$ (LRFF/MRFF)	075 (decreases upward: decrease of LREE enrichment)	0.77 (intense decreases upward: decrease of LREE enrichment)		Nothdruft et al. (2004)
(Sm/Yb)$_{PAAS}$ (MRFF/HRFF)	1.45 (increases upward: increase of LREE enrichment)	1.55 (slightly increases upward: increase of LREE enrichment)		Nothdruft et al. (2004)
La vs. Ce	3.36 (increases upward: enrichment of Ce --> biogenic, terrigenous)	3.27 (increases upward: enrichment of Ce --> biogenic, terrigenous)		Toth (1980)
Y/Ho	22.29 (decreases upward: terrigenous effect, increase of adsorption)	29.31 (decreases upward: terrigenous effect, increase of adsorption)		Song et al. (2012)
Y/Ho vs. La	Terrigenous effect exist	Terrigenous effect exist		Song et al. (2012)

$(La/Yb)_{PAAS}$ vs. $(La/Sm)_{PAAS}$	via early diagenesis: adsorption	via early diagenesis: adsorption		Bau and Dulski (1996)
Sm/Yb vs. Eu/Sm, Y/Ho vs. Eu/Sm, Y/Ho vs. Sm/Yb	no direct hydrothermal effect	no direct hydrothermal effect		Bau and Dulski (1996)
Zr/Rb	near 1 - fine grained sediments without Q input	1.32		Dypvik and Harris (2001)
Rb/Cs	15±4 - fine grained sediments	16.74		Scheffler (2004)
Zr/Ti	0.03 - neutral magmatic rocks provenance area	0.03		Scheffler (2004)
Rb/K	0.002-0.003: fresh water input	0.003		Campbell and Williams (1965)
Co/Cr, Ni/Co, Co/Ni, U/Th V/Cr	oxygenic conditions	oxygenic conditions		Algeo and Maynard (2004)
V/(V+Ni)	Suboxic conditions (microbial mediation!)	suboxic		Algeo and Maynard (2004)
(Cu+Mo)/Zn	suboxic condition (microbial mediation!)	suboxic condition (microbial mediation!)		Algeo and Maynard (2004)
CIA	≤50 fresh, not weathered, FP17-FP25A: CIA 50-60 slight weathering rate	<50		Nesbitt and Young (1982)

B	**Black shale (Úrkút)**	**Posidonia Shale**	João et al. (2012)
Proxy			
Enrichment factor (EF median)	Te, Co, S, As, Mn, Mo, Ca > 5	S, Sc > 5	
	In, Hf, K, Ba, Na < 1	Sb, Rb, Ba, Ti, Zr, Mg, K, Na, Mn < 1	
	Max.: Co 15.0; (Te 17.4)	Max: S 11.5	
Paleoredox			
Ni/Co	Oxic	Oxic	
V/Cr	Oxic-Suboxic	Oxic	
V/(V+Ni)	Suboxic	Anoxic	
$Mn^* = \log[(Mn/Mn_{PAAS})/(Fe/Fe_{PAAS})]$	Oxic-Suboxic	Sub-Anoxic	

Table 4. Organic geochemical and isotopic data

Sample ID		Elevation (m)	TOC (wt. %)	N (wt. %)	C (wt. %)	C/N	S1 (mgCH/ g rock)	S2 (mgCH/ g rock)	HI (mgCH/ g TOC)	T_{max} (°C)	$\delta^{13}C_{carb}$ ‰ V-PDB	$\delta^{18}O_{carb}$ ‰ V-SMOW	$\delta^{13}C_{org}$ ‰ V-PDB
FP21	Bs3-4	25.2	1.73	0.08	5.79	22.0	0.11	2.98	172	423	-4.0	-2.6	-30.6
FP22D		24.3	0.85	0.05	4.76	17.3	0.05	0.75	88	426	-9.1	-1.3	-30.8
FP22C		24.2	0.61	0.03	2.23	22.9	0.04	0.43	69	423	-7.7	-2.8	-29.9
FP22B		24.2	1.07	0.05	7.05	22.7	0.06	0.63	59	428	-9.4	-0.6	-30.7
FP22A		24.2	1.27	0.06	6.92	23.0	0.05	0.70	55	427	-10.0	-0.8	-30.8
Z/1		23.9	1.06	0.05	4.90	20.2	0.10	1.37	128	425	-8.1	-1.9	-
Z/2		23.7	1.24	0.06	5.90	20.1	0.08	1.59	129	422	-8.1	-1.4	-
Min			0.61	0.03	2.23	17.3	0.04	0.43	55	422	-10.0	-2.8	-30.8
Max			1.73	0.08	7.05	23.0	0.11	2.98	172	428	-4.0	-0.6	-29.9
Average			1.12	0.05	5.36	21.2	0.07	1.21	100	425	-8.0	-1.6	-30.6
Median			1.07	0.05	5.79	22.0	0.06	0.75	88	425	-8.1	-1.4	-30.7
FP9	Bs2	-	-	-	-	-	-	-	-	-	-	-	-32.0
FP10		-	-	-	-	-	-	-	-	-	-	-	-31.8
Z/10'''		-	-	-	-	-	-	-	-	-	-	-	-
Z/10''		18.4	2.79	0.11	4.58	24.7	0.18	8.90	319	420	-2.8	-4.1	-
Z/10'		-	-	-	-	-	-	-	-	-	-	-	-
Z/15		17.7	3.53	0.13	5.49	26.2	0.27	17.30	490	419	-4.8	-3.9	-
FP24B		12.3	3.11	0.12	5.85	26.7	0.15	13.30	428	422	-3.5	-3.4	-32.6
FP24A		12.2	2.41	0.10	4.69	24.5	0.13	9.42	391	419	-3.5	-3.4	-32.6
FP11		-	-	-	-	-	-	-	-	-	-	-	-32.9
5/19		11.5	1.84	0.08	2.28	23.2	-	-	193	411	-5.1	-2.2	-
FP7		-	-	-	-	-	-	-	-	-	-	-	-32.4
FP6		-	-	-	-	-	-	-	-	-	-	-	-31.9
FP5		-	-	-	-	-	-	-	-	-	-	-	-31.8
5/18		11.2	1.90	0.09	2.16	21.1	0.10	2.33	123	410	-6.6	-3.4	
FP4		-	-	-	-	-	-	-	-	-	-	-	-32.7
FP3		-	-	-	-	-	-	-	-	-	-	-	-32.7
5/17		10.9	1.79	0.08	2.26	21.9	0.12	2.84	158	415	-4.9	-2.0	-
FP23B2		10.8	1.44	0.07	2.95	21.2	0.08	2.70	188	421	-3.3	-2.6	-32.8
FP23B1		10.7	1.46	0.07	2.92	21.9	0.08	3.30	226	419	-3.5	-2.6	-32.8
FP23A		10.7	0.56	0.04	5.87	13.8	0.04	0.49	87	415	-18.1	-1.7	-32.0
Min			0.56	0.04	2.16	13.8	0.04	0.49	87	410	-18.1	-4.1	-32.9
Max			3.53	0.13	5.87	26.7	0.27	17.30	490	422	-2.8	-1.7	-31.8
Average			2.08	0.09	3.90	22.5	0.13	6.73	260	417	-5.6	-2.9	-32.5
Median			1.87	0.09	3.76	22.6	0.12	3.30	209	419	-4.1	-3.0	-32.6
FP19	Bs1	0.6	0.91	0.03	6.40	31.5	0.04	0.37	41	443	-9.0	0.7	-30.5
FP18B		0.5	0.76	0.04	4.91	18.3	0.03	0.49	64	423	-7.5	0.7	-32.9
FP18A		0.5	0.96	0.05	4.26	19.4	0.05	0.66	68	425	-9.8	0.1	-33.4
FP17		0.3	1.06	0.06	1.69	18.1	0.05	0.93	88	423	-5.8	-1.8	-33.6
FP16B		0.3	0.86	0.04	4.70	20.8	0.05	0.74	86	422	-6.1	0.5	-33.1
FP16A		0.2	0.74	0.04	4.04	16.6	0.03	0.78	106	421	-5.9	0.9	-32.5
FP16		0.2	0.59	0.04	4.50	15.1	0.04	0.41	70	423	-6.1	1.1	-32.8
FP15		0.1	0.85	0.06	1.96	14.0	0.04	0.65	76	421	-5.1	-1.3	-32.6
FP8		0.05	-	-	-	-	-	-	-	-	-	-	-33.3
Min			0.59	0.03	1.69	14.01	0.03	0.37	41	421	-9.8	-1.8	-33.6
Max			1.06	0.06	6.40	31.50	0.05	0.93	106	443	-5.1	1.1	-30.5
Average			0.84	0.05	4.06	19.23	0.04	0.63	75	425	-6.9	0.1	-32.7
Median			0.85	0.04	4.38	18.22	0.04	0.65	73	423	-6.1	0.6	-32.9

Table 5. Effects and calculation on accumulation based on mineralogy

Legend	Process	Minerals used for calculation	Minerals used for calculation
a	**Starved basin, lack of terrestrial detrial input**	**Authigenesis**	**Allochtonous**
		q/2*, sid, bar, zeol, smec, cel, dol, rhod, pyr, cal/2**	chl, kaol, clay, plag, K-fp, q/2, cal/2
b	**Ore forming processes**	**Ore forming minerals**	**Non-ore forming**
		sid, smec, cel, rhod	bar, zeol, pyr, kut, chl, kaol, clay, plag, K-fp, dol, cal, q
c	**Background black shale sedimentation**	**Early diagenetic**	**Original non diagenetic**
	Ore forming minerals not considered here	2q/3, cal/2, pyr, zeol, bar, dol, kut	q/3, chl, kaol, clay, plag, K-fp, cal/2
d	**Effect of diagenesis**	**Diagenetic**	**Non diagenetic**
		q/2, rhod, kut, pyr, zeol, bar, sid, dol, cal/2	q/2, chl, kaol, clay, cel, smec, plag, K-fp, cal/2
e/1	**Effect of microbial mediation (with pyrite)**	**Biogenic (with pyrite)**	**Non biogenic**
		rhod, sid, pyr, q/2, dol, smec, cel	bar, zeol, kut, chl, kaol, clay, plag, K-fp, q/2
e/2	**Effect of microbial mediation (no pyrite)**	**Biogenic (no pyrite)**	**Non biogenic**
	cal/2 as biodebris not considered here	rhod, sid, q/2, dol, smec, cel, cal/2	bar, zeol, kut, chl, kaol, clay, plag, K-fp, q/2
f	**Ash contribution**	**Ash contribution**	**All others**
		q/3, plag, K-fp	2q/3, smec, cel, chl, kaol, clay, sid, cal, rhod, kut, pyr, zeol, bar, dol
g	**Windblown contribution**	**Windblown**	**All others**
		q/3	2q/3, plag, K-fp, smec, cel, chl, kaol, clay, sid, cal, rhod, kut, pyr, zeol, bar, dol
h	**Biodebris contribution**	**Biodebris**	**Non biodebris**
		q/3, cal	2q/3, plag, K-fp, smec, cel, chl, kaol, clay, sid, rhod, kut, pyr, zeol, bar, dol

See text for origin of the different minerals, and Figs. 7 and 8.

q-quartz; plag-plagioclase, K-fp-K-feldspar; smec-smectite; cel-celadonite; chl-chlorite; kaol-kaolinite; clay-not determined in detail; sid-siderite; cal-calcite; rhod-rhodochrosite; kut-kutnohorite; pyr-pyrite; zeol-zeolite; bar-barite; dol-dolomite; clay-unspecified clay minerals

Figure 1

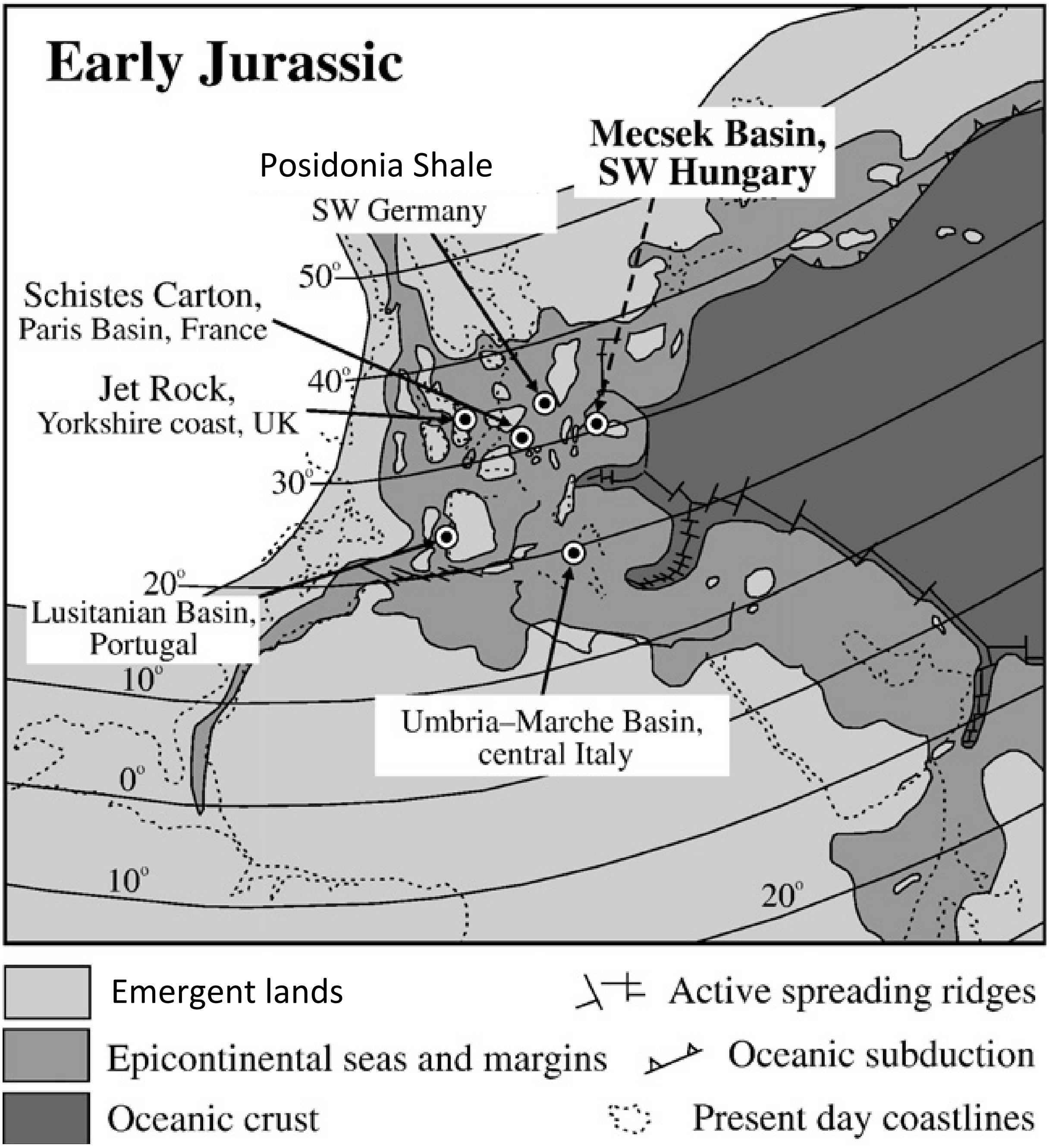
Early Jurassic
Mecsek Basin, SW Hungary
Posidonia Shale
SW Germany
Schistes Carton, Paris Basin, France
Jet Rock, Yorkshire coast, UK
Lusitanian Basin, Portugal
Umbria–Marche Basin, central Italy
50°
40°
30°
20°
10°
0°
10°
20°
Emergent lands
Epicontinental seas and margins
Oceanic crust
Active spreading ridges
Oceanic subduction
Present day coastlines

Figure 2

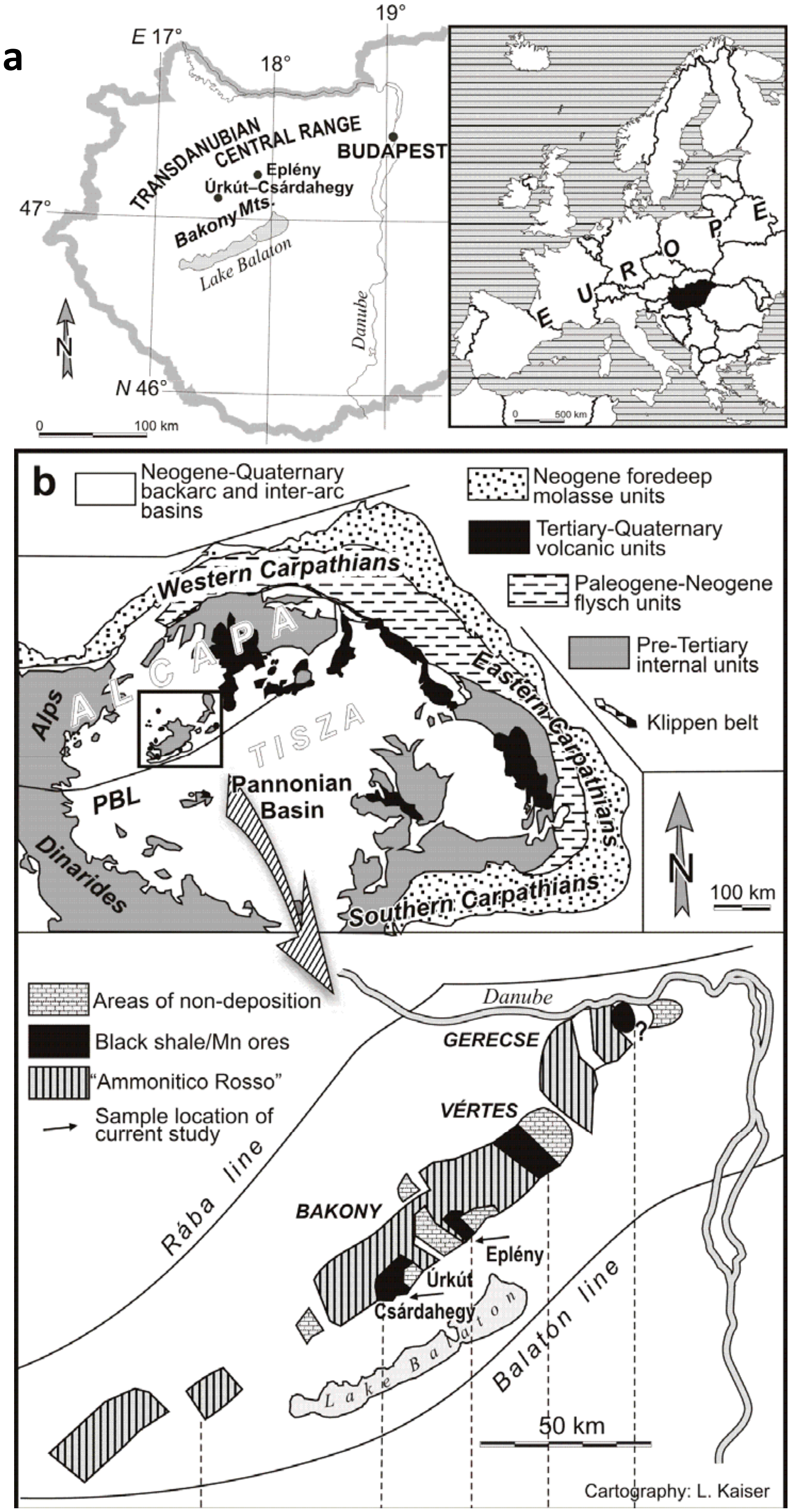
a
E 17°
18°
19°
47°
N 46°
TRANSDANUBIAN CENTRAL RANGE
BUDAPEST
Eplény
Úrkút–Csárdahegy
Bakony Mts.
Lake Balaton
Danube
N
0
100 km
E U R O P E
0
500 km
b
Neogene-Quaternary backarc and inter-arc basins
Neogene foredeep molasse units
Tertiary-Quaternary volcanic units
Paleogene-Neogene flysch units
Pre-Tertiary internal units
Klippen belt
Western Carpathians
A L C A P A
Alps
T I S Z A
Pannonian Basin
PBL
Dinarides
Eastern Carpathians
Southern Carpathians
N
100 km
Areas of non-deposition
Black shale/Mn ores
"Ammonitico Rosso"
Sample location of current study
Danube
GERECSE
?
VÉRTES
BAKONY
Eplény
Úrkút
Csárdahegy
Rába line
Balatón line
Lake Balaton
50 km
Cartography: L. Kaiser

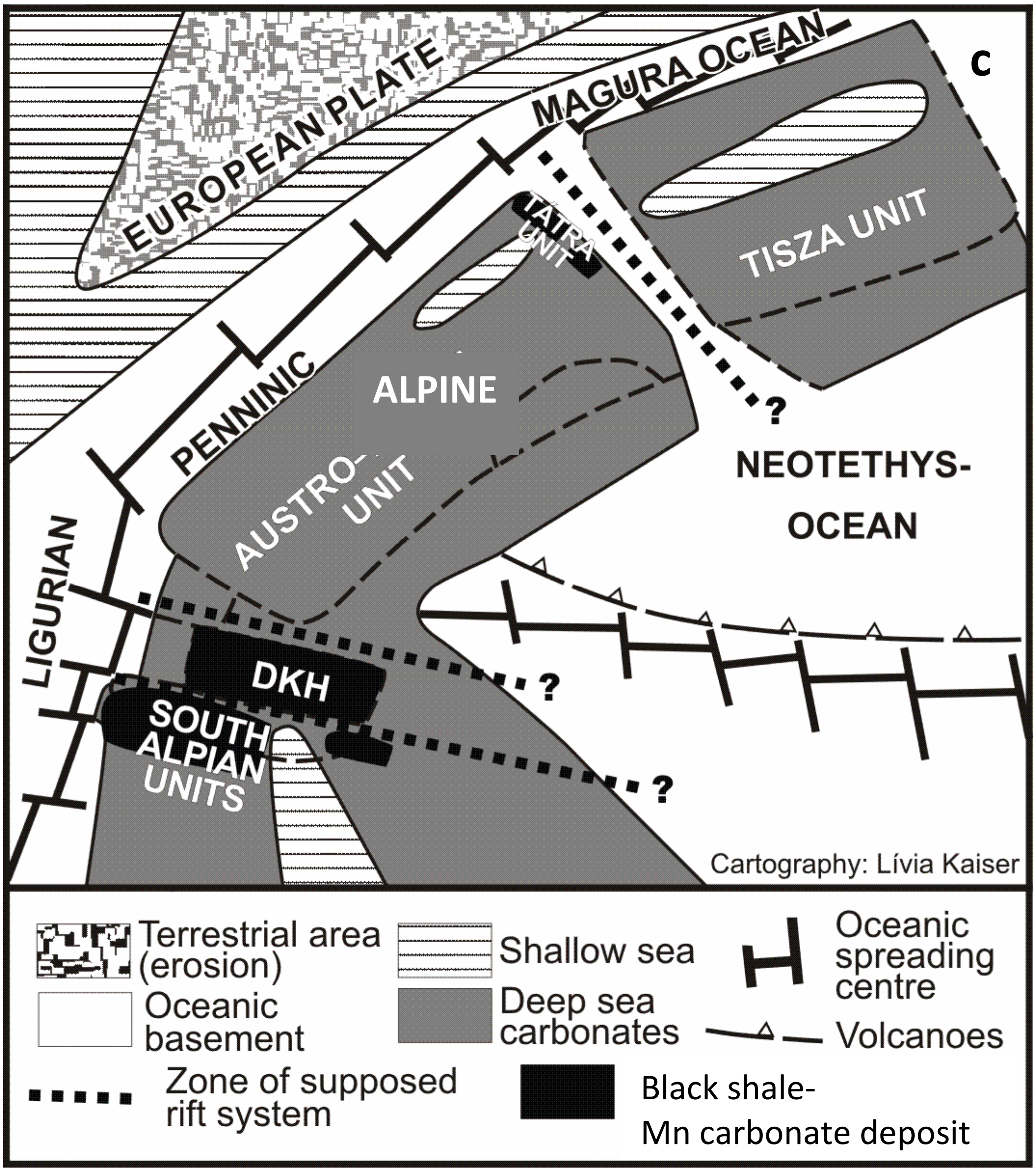

Cartography: Lívia Kaiser

Figure 3

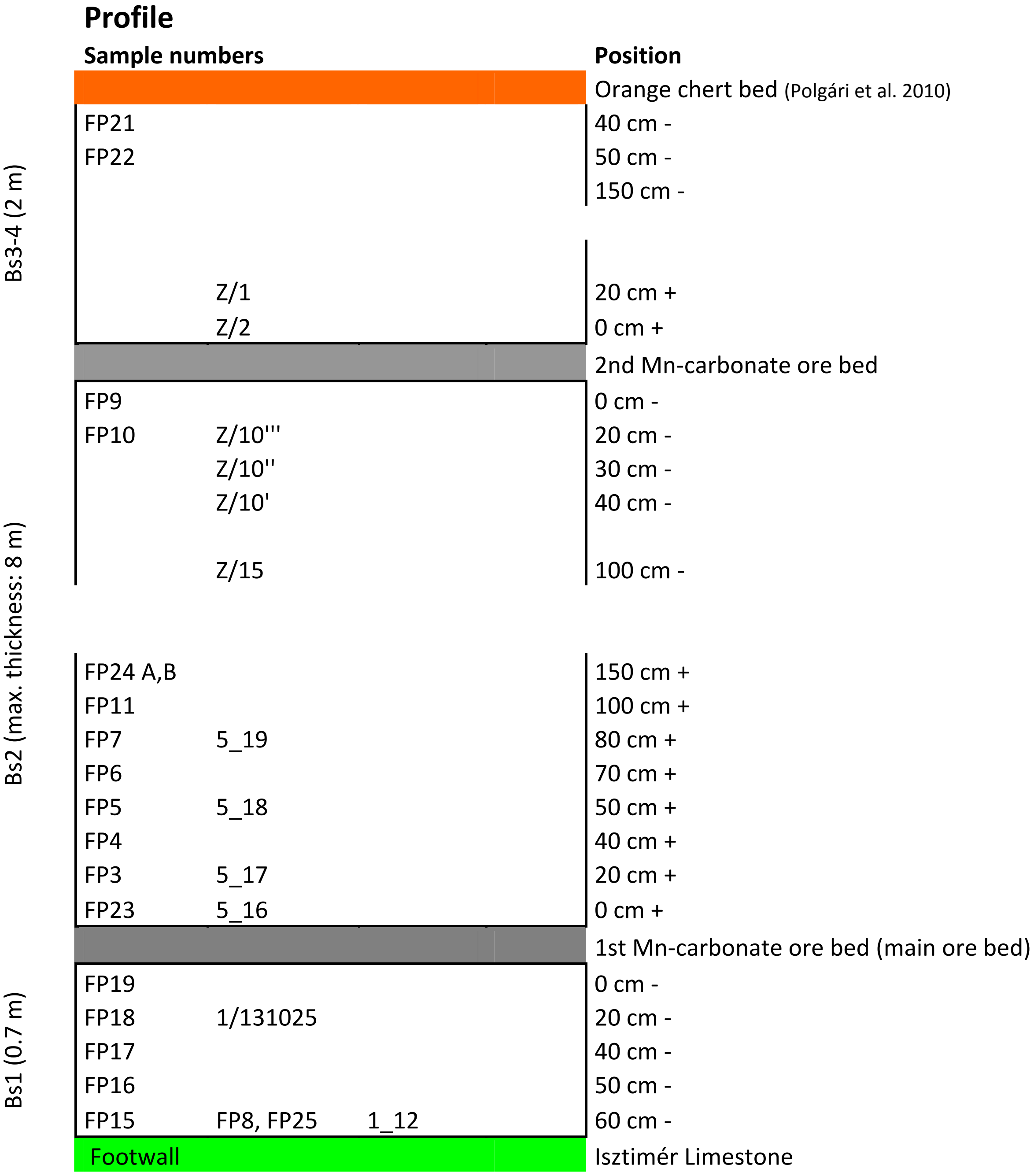

Profile

	Sample numbers			Position
	🟧			Orange chert bed (Polgári et al. 2010)
Bs3-4 (2 m)	FP21			40 cm -
	FP22			50 cm -
				150 cm -
		Z/1		20 cm +
		Z/2		0 cm +
	▨			2nd Mn-carbonate ore bed
Bs2 (max. thickness: 8 m)	FP9			0 cm -
	FP10	Z/10'''		20 cm -
		Z/10''		30 cm -
		Z/10'		40 cm -
		Z/15		100 cm -
	FP24 A,B			150 cm +
	FP11			100 cm +
	FP7	5_19		80 cm +
	FP6			70 cm +
	FP5	5_18		50 cm +
	FP4			40 cm +
	FP3	5_17		20 cm +
	FP23	5_16		0 cm +
	▨			1st Mn-carbonate ore bed (main ore bed)
Bs1 (0.7 m)	FP19			0 cm -
	FP18	1/131025		20 cm -
	FP17			40 cm -
	FP16			50 cm -
	FP15	FP8, FP25	1_12	60 cm -
	🟩 Footwall			Isztimér Limestone

Figure 4

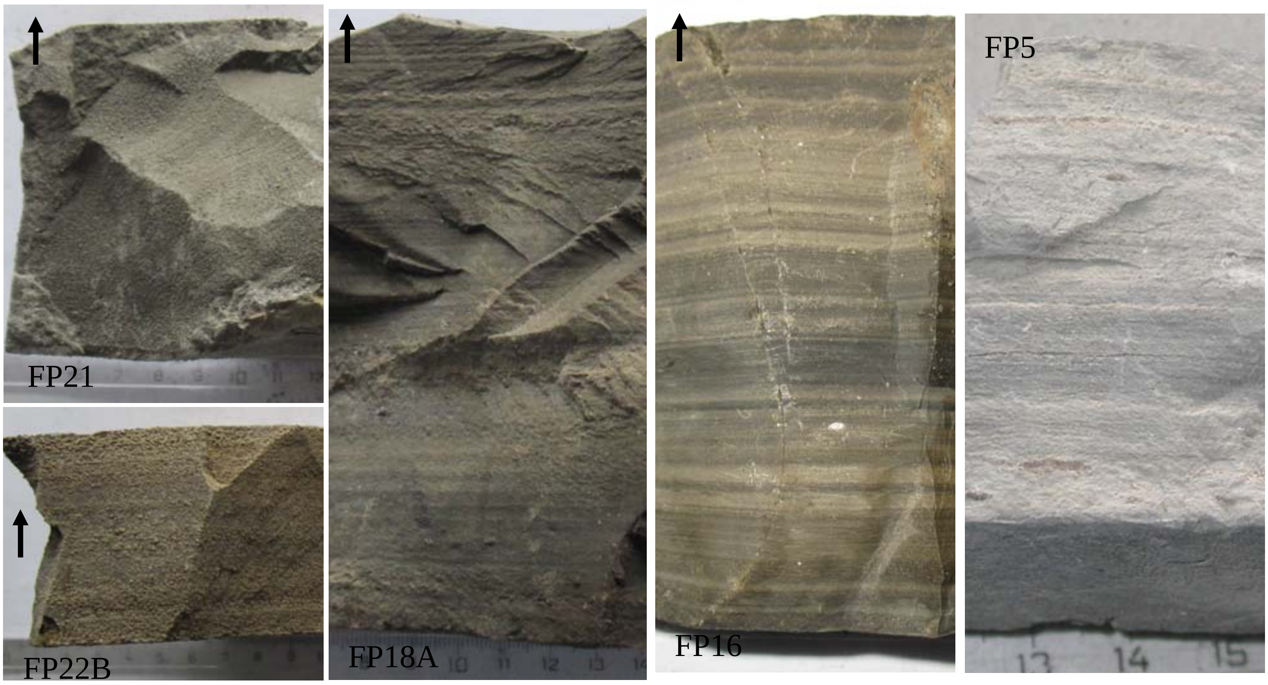

Figure 5

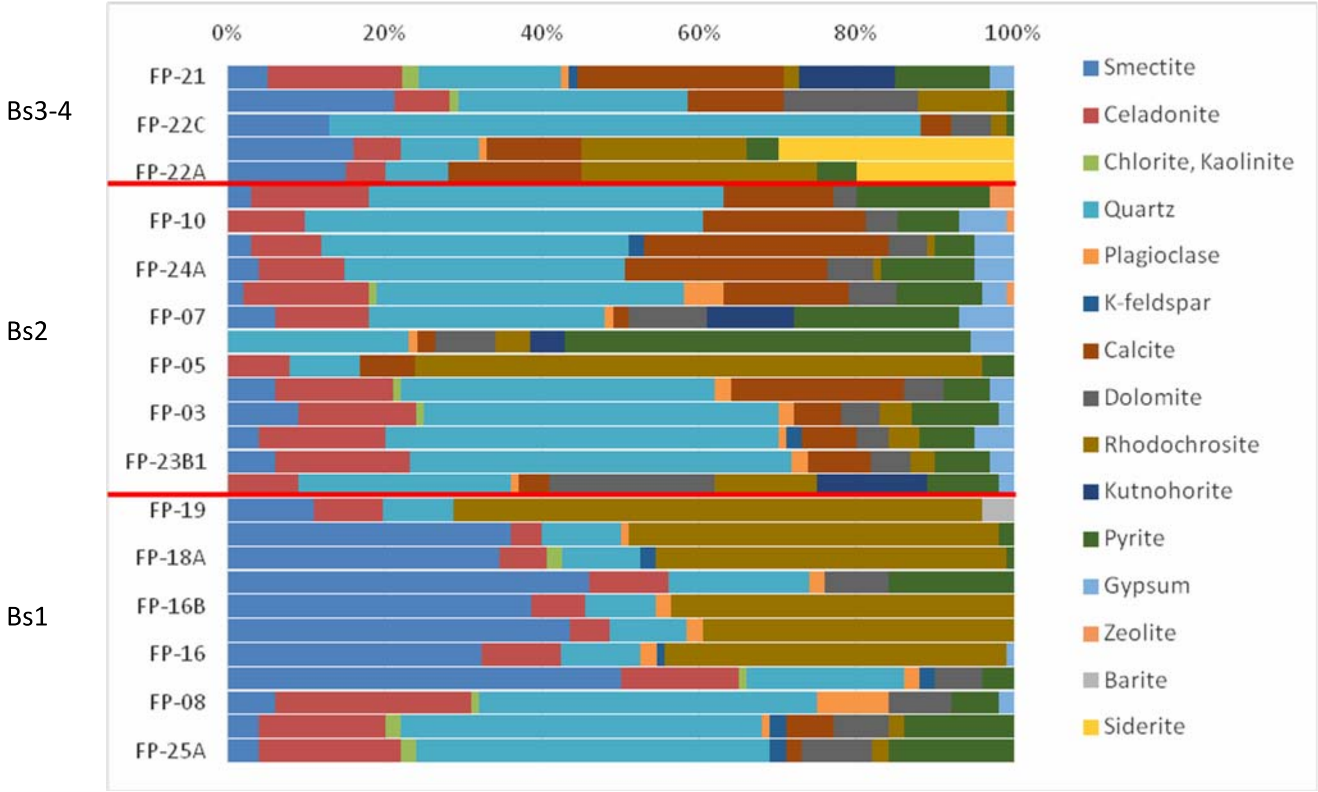
0%
20%
40%
60%
80%
100%
Bs3-4
Bs2
Bs1
FP-21
FP-22C
FP-22A
FP-10
FP-24A
FP-07
FP-05
FP-03
FP-23B1
FP-19
FP-18A
FP-16B
FP-16
FP-08
FP-25A
Smectite
Celadonite
Chlorite, Kaolinite
Quartz
Plagioclase
K-feldspar
Calcite
Dolomite
Rhodochrosite
Kutnohorite
Pyrite
Gypsum
Zeolite
Barite
Siderite

Figure 6

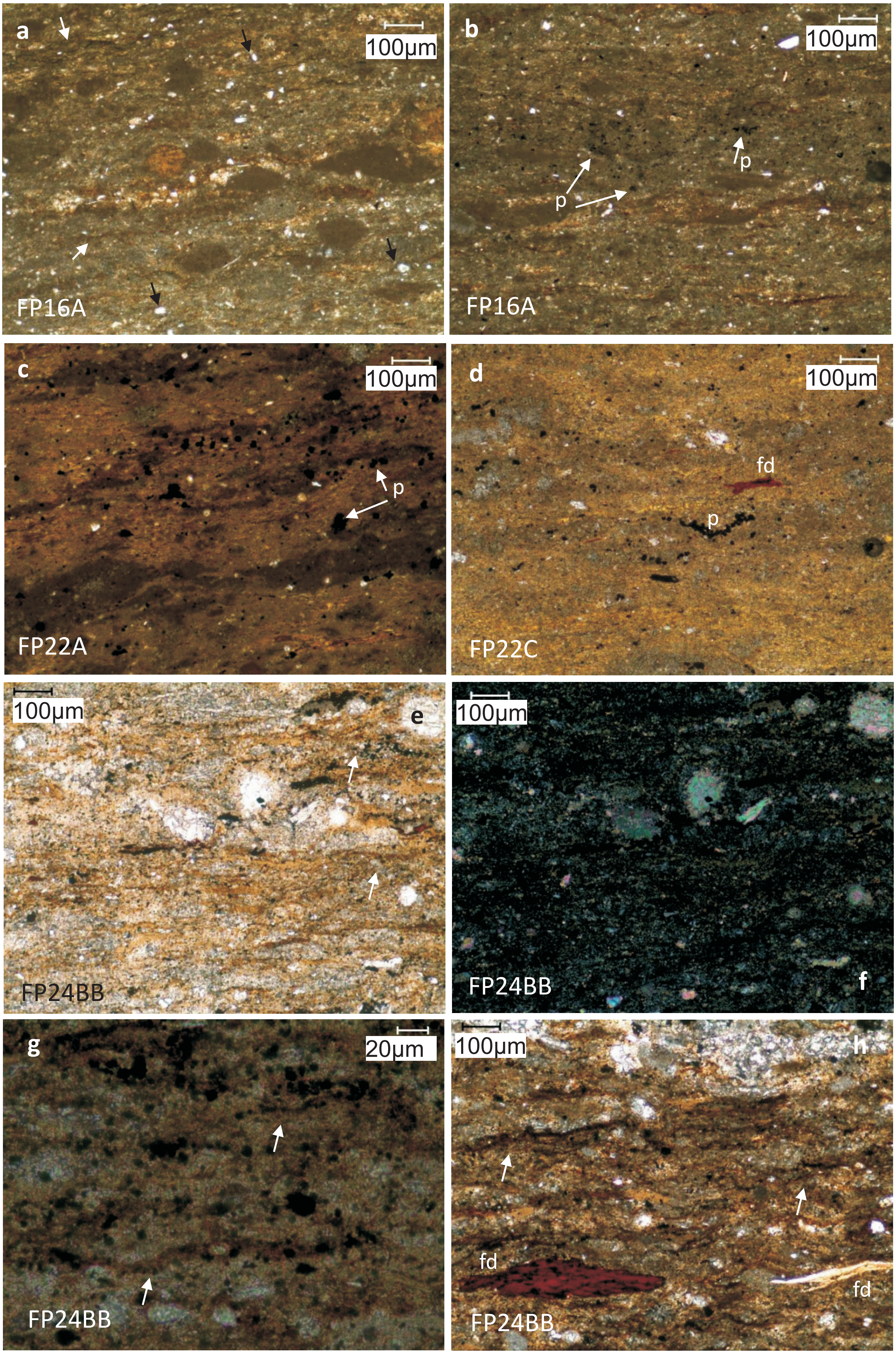
a
100µm
FP16A
b
100µm
p
p
FP16A
c
100µm
p
FP22A
d
100µm
fd
p
FP22C
100µm
e
FP24BB
100µm
FP24BB
f
g
20µm
FP24BB
100µm
h
fd
fd
FP24BB

Figure 7

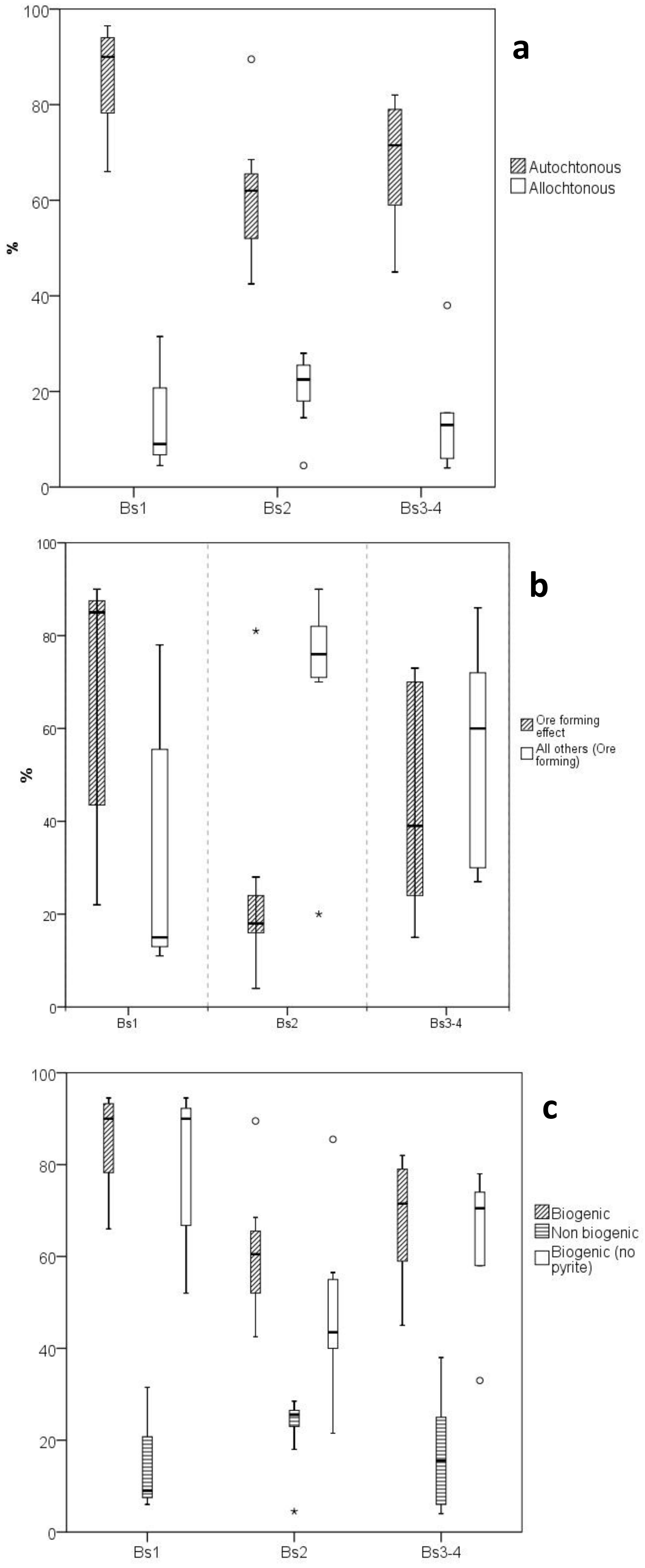
a
%
0
20
40
60
80
100
Bs1
Bs2
Bs3-4
▨ Autochtonous
☐ Allochtonous
b
%
0
20
40
60
80
100
Bs1
Bs2
Bs3-4
▨ Ore forming effect
☐ All others (Ore forming)
c
0
20
40
60
80
100
Bs1
Bs2
Bs3-4
▨ Biogenic
▤ Non biogenic
☐ Biogenic (no pyrite)

Figure 8

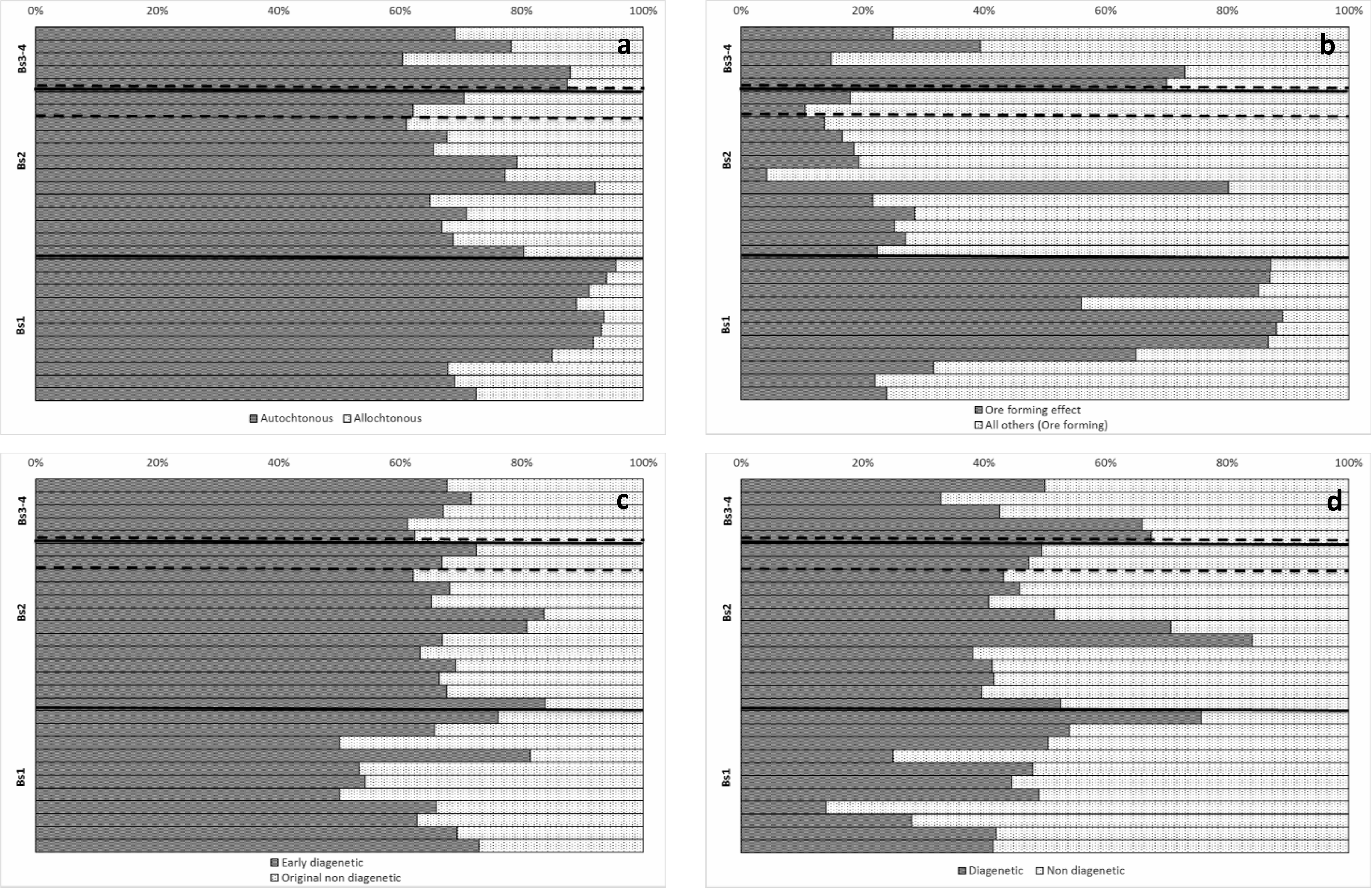

0%
20%
40%
60%
80%
100%
a
b
c
d
Bs3-4
Bs2
Bs1
▨ Autochtonous ☐ Allochtonous
▨ Ore forming effect
☐ All others (Ore forming)
▨ Early diagenetic
☐ Original non diagenetic
▨ Diagenetic ☐ Non diagenetic

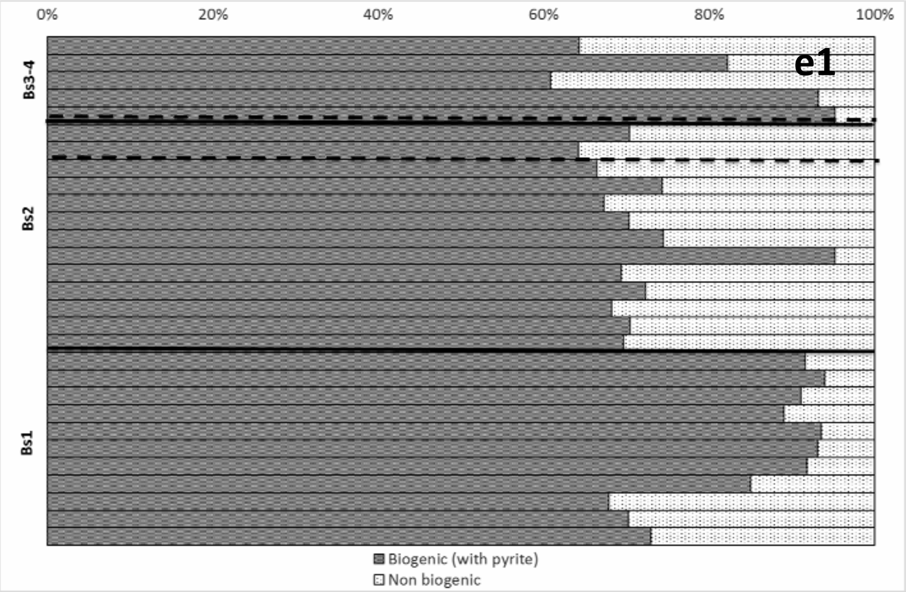
e1
0%
20%
40%
60%
80%
100%
Bs3-4
Bs2
Bs1
▨ Biogenic (with pyrite)
▨ Non biogenic

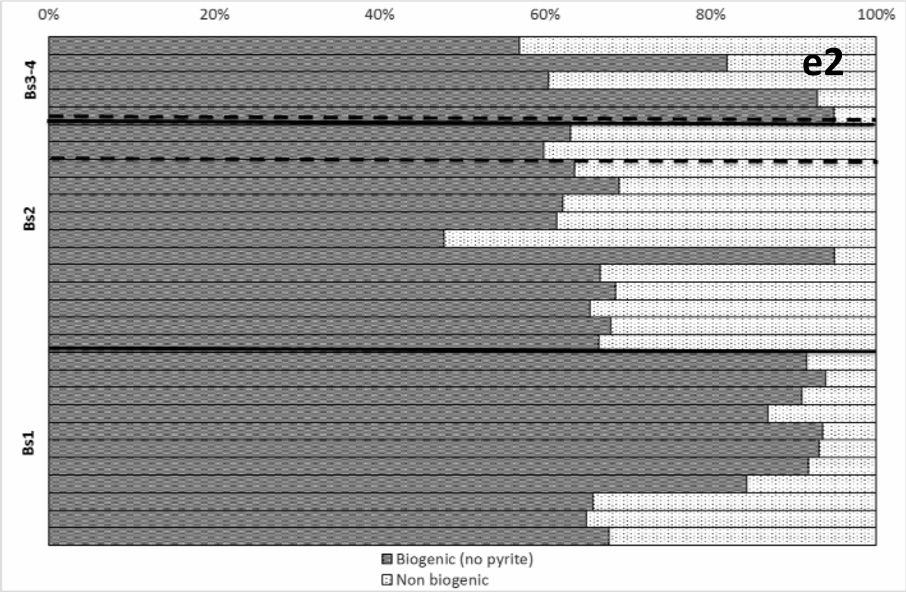
e2
0%
20%
40%
60%
80%
100%
Bs3-4
Bs2
Bs1
▨ Biogenic (no pyrite)
▨ Non biogenic

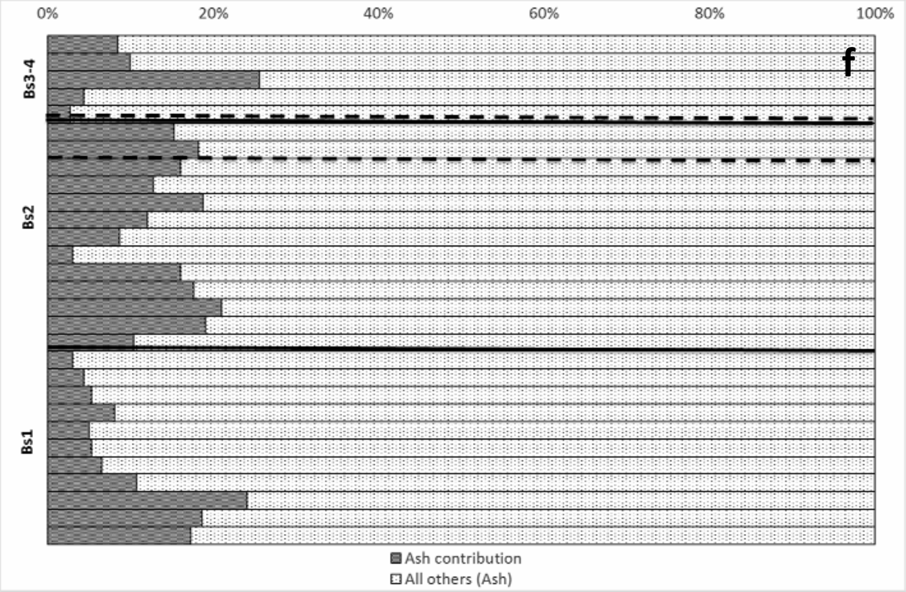
f
0%
20%
40%
60%
80%
100%
Bs3-4
Bs2
Bs1
▨ Ash contribution
▨ All others (Ash)

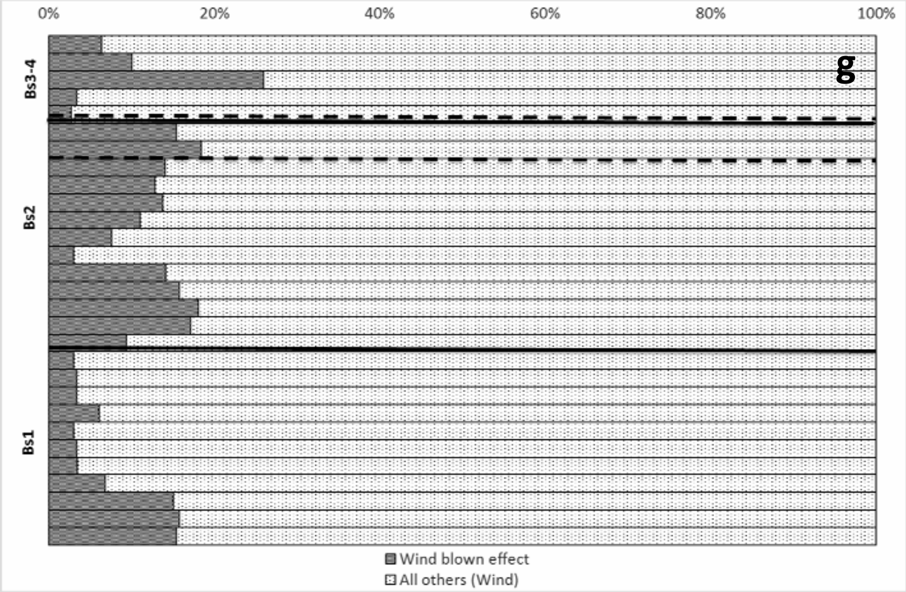
g
0%
20%
40%
60%
80%
100%
Bs3-4
Bs2
Bs1
▨ Wind blown effect
▨ All others (Wind)

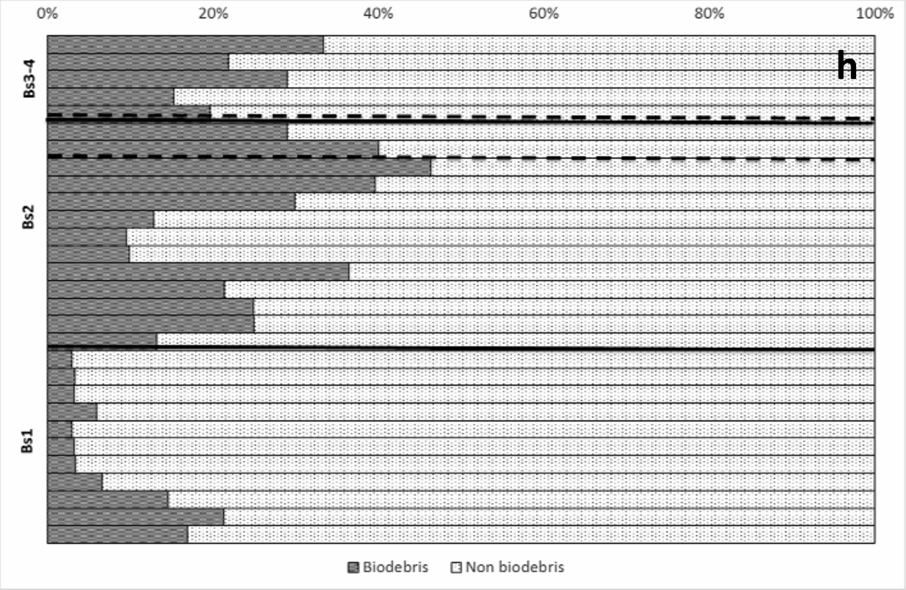
0%
20%
40%
60%
80%
100%
h
Bs3-4
Bs2
Bs1
Biodebris
Non biodebris

Figure 9

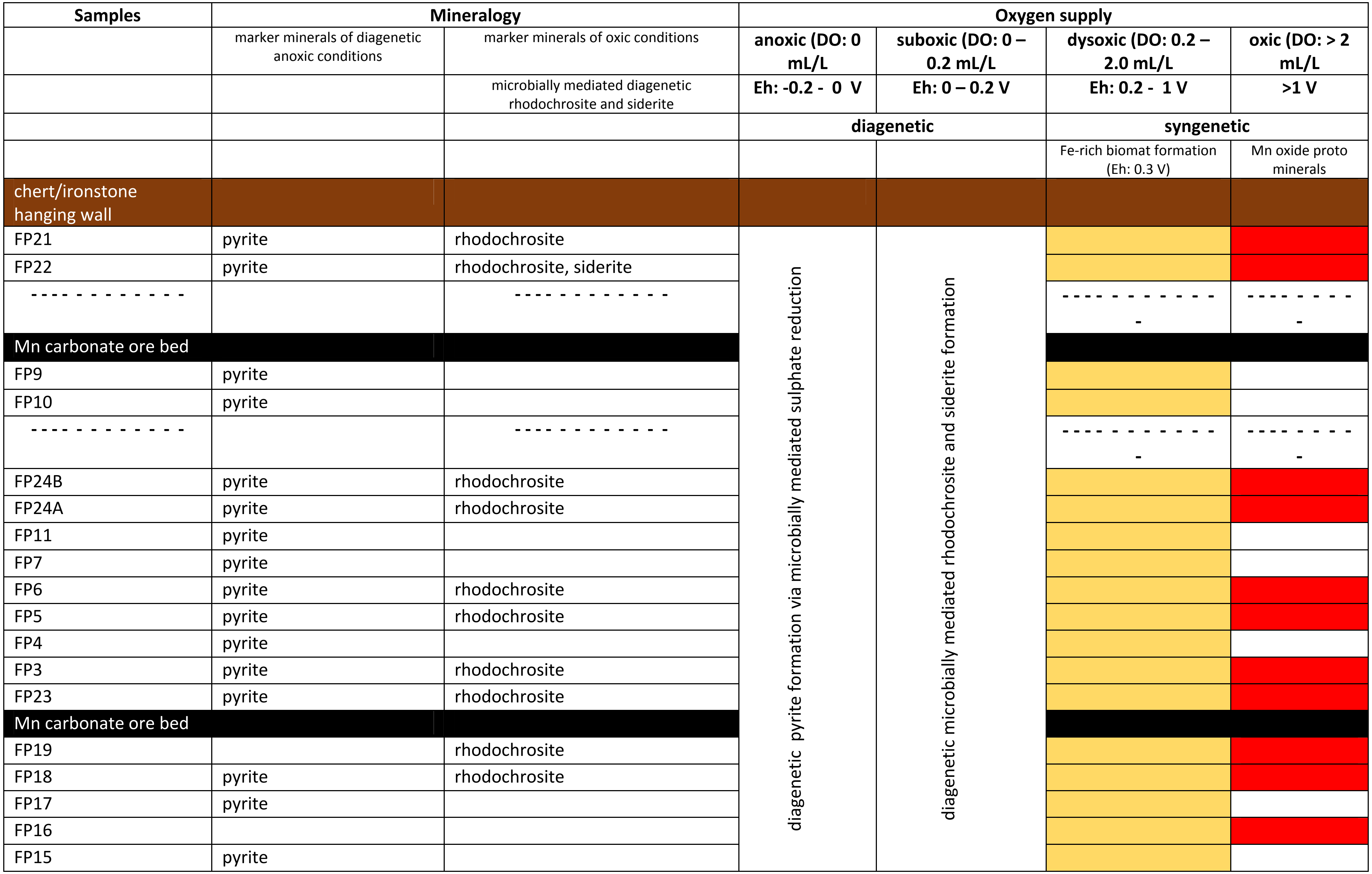

Samples	Mineralogy		Oxygen supply			
	marker minerals of diagenetic anoxic conditions	marker minerals of oxic conditions	**anoxic (DO: 0 mL/L**	**suboxic (DO: 0 – 0.2 mL/L**	**dysoxic (DO: 0.2 – 2.0 mL/L**	**oxic (DO: > 2 mL/L**
		microbially mediated diagenetic rhodochrosite and siderite	**Eh: -0.2 - 0 V**	**Eh: 0 – 0.2 V**	**Eh: 0.2 - 1 V**	**>1 V**
			diagenetic		**syngenetic**	
					Fe-rich biomat formation (Eh: 0.3 V)	Mn oxide proto minerals
chert/ironstone hanging wall						
FP21	pyrite	rhodochrosite	diagenetic pyrite formation via microbially mediated sulphate reduction	diagenetic microbially mediated rhodochrosite and siderite formation	🟨	🟥
FP22	pyrite	rhodochrosite, siderite			🟨	🟥
- - - - - - - - - - - -		- - - - - - - - - - - -			- - - - - - - - - - - -	- - - - - - - - -
Mn carbonate ore bed						
FP9	pyrite				🟨	
FP10	pyrite				🟨	
- - - - - - - - - - - -		- - - - - - - - - - - -			- - - - - - - - - - - -	- - - - - - - - -
FP24B	pyrite	rhodochrosite			🟨	🟥
FP24A	pyrite	rhodochrosite			🟨	🟥
FP11	pyrite				🟨	
FP7	pyrite				🟨	
FP6	pyrite	rhodochrosite			🟨	🟥
FP5	pyrite	rhodochrosite			🟨	🟥
FP4	pyrite				🟨	
FP3	pyrite	rhodochrosite			🟨	🟥
FP23	pyrite	rhodochrosite			🟨	🟥
Mn carbonate ore bed						
FP19		rhodochrosite			🟨	🟥
FP18	pyrite	rhodochrosite			🟨	🟥
FP17	pyrite				🟨	
FP16					🟨	🟥
FP15	pyrite				🟨	

Figure 10

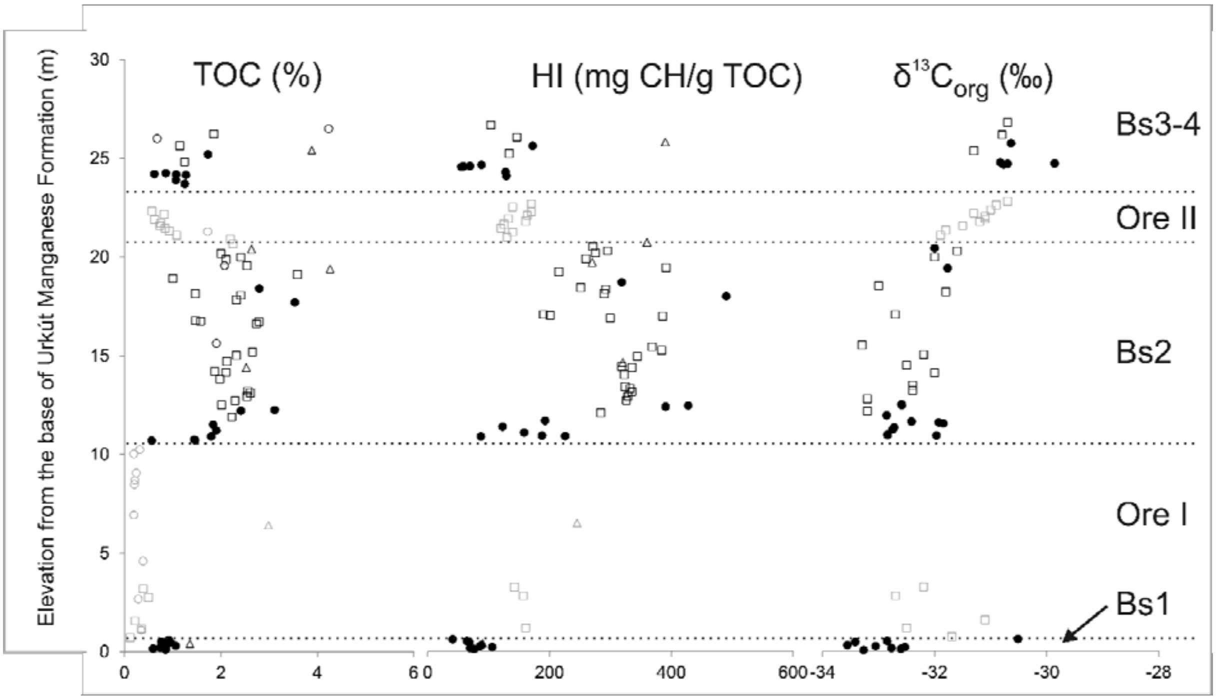

Elevation from the base of Urkút Manganese Formation (m)
30
25
20
15
10
5
0
TOC (%)
0
2
4
6
HI (mg CH/g TOC)
0
200
400
600
$\delta^{13}C_{org}$ (‰)
-34
-32
-30
-28
Bs3-4
Ore II
Bs2
Ore I
Bs1

Figure 11

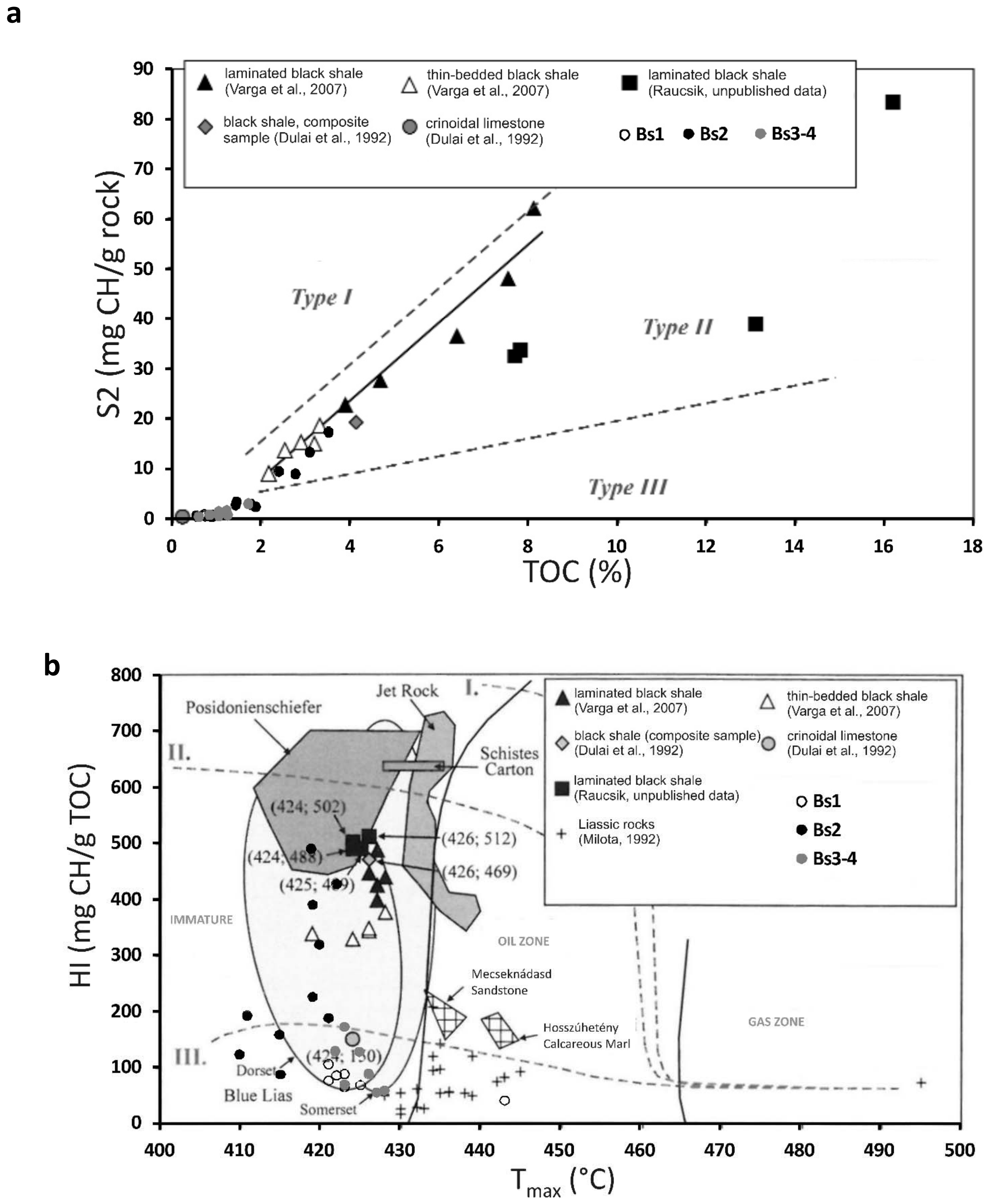

a
S2 (mg CH/g rock)
90
80
70
60
50
40
30
20
10
0
laminated black shale (Varga et al., 2007)
thin-bedded black shale (Varga et al., 2007)
laminated black shale (Raucsik, unpublished data)
black shale, composite sample (Dulai et al., 1992)
crinoidal limestone (Dulai et al., 1992)
○ Bs1 ● Bs2 ● Bs3-4
Type I
Type II
Type III
0
2
4
6
8
10
12
14
16
18
TOC (%)
b
HI (mg CH/g TOC)
800
700
600
500
400
300
200
100
0
Posidonienschiefer
Jet Rock
I.
II.
III.
Schistes Carton
(424; 502)
(424; 488)
(425; 489)
(426; 512)
(426; 469)
(424; 130)
IMMATURE
OIL ZONE
GAS ZONE
Mecseknádasd Sandstone
Hosszúhetény Calcareous Marl
Dorset
Blue Lias
Somerset
laminated black shale (Varga et al., 2007)
thin-bedded black shale (Varga et al., 2007)
black shale (composite sample) (Dulai et al., 1992)
crinoidal limestone (Dulai et al., 1992)
laminated black shale (Raucsik, unpublished data)
Liassic rocks (Milota, 1992)
○ Bs1
● Bs2
● Bs3-4
400
410
420
430
440
450
460
470
480
490
500
T_{max} (°C)

Figure 12

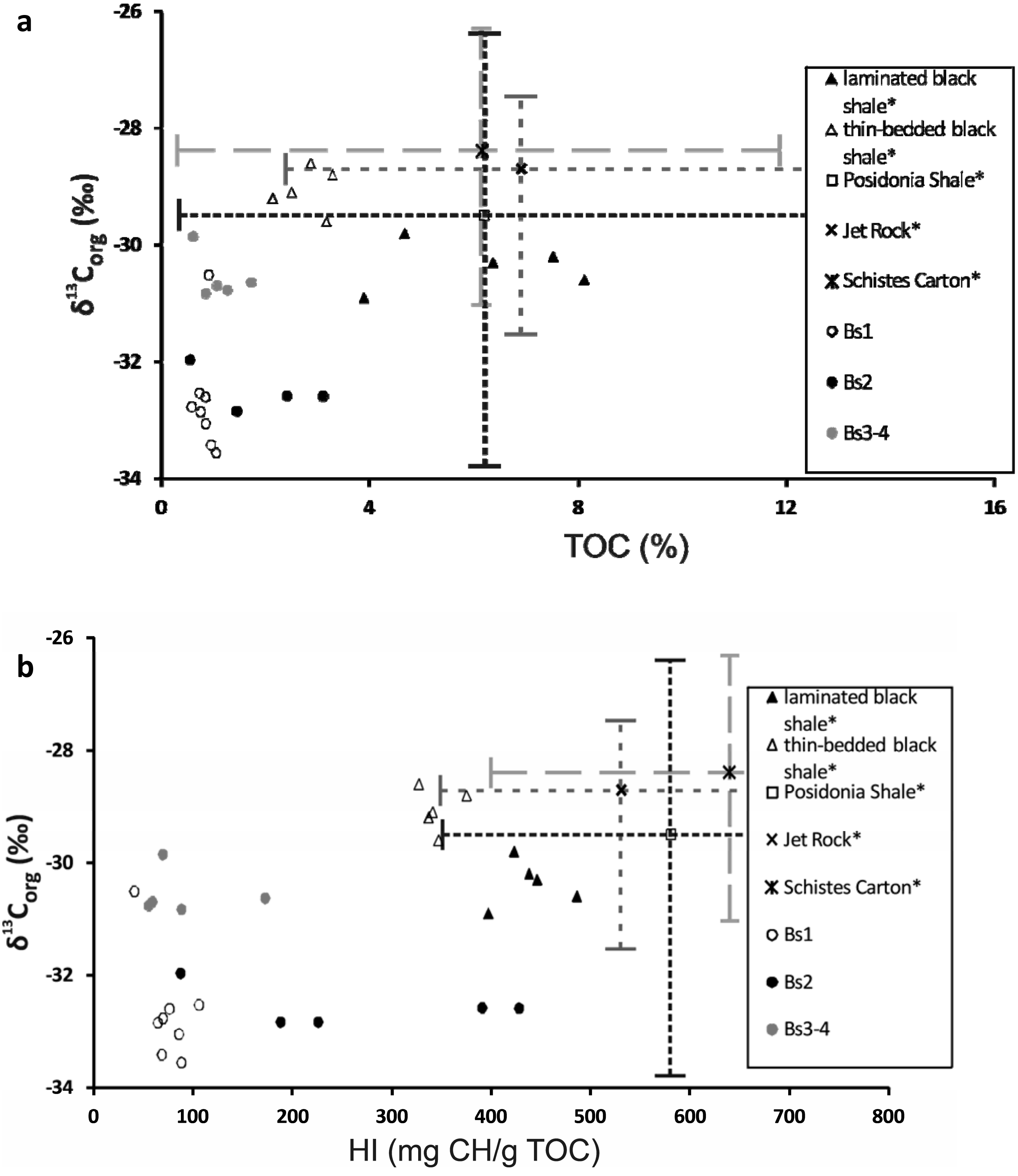
a
-26
-28
-30
-32
-34
δ^{13}C$_{org}$ (‰)
0
4
8
12
16
TOC (%)
▲ laminated black shale*
△ thin-bedded black shale*
□ Posidonia Shale*
× Jet Rock*
⋇ Schistes Carton*
○ Bs1
● Bs2
● Bs3-4
b
-26
-28
-30
-32
-34
δ^{13}C$_{org}$ (‰)
0
100
200
300
400
500
600
700
800
HI (mg CH/g TOC)
▲ laminated black shale*
△ thin-bedded black shale*
□ Posidonia Shale*
× Jet Rock*
⋇ Schistes Carton*
○ Bs1
● Bs2
● Bs3-4

Figure 13

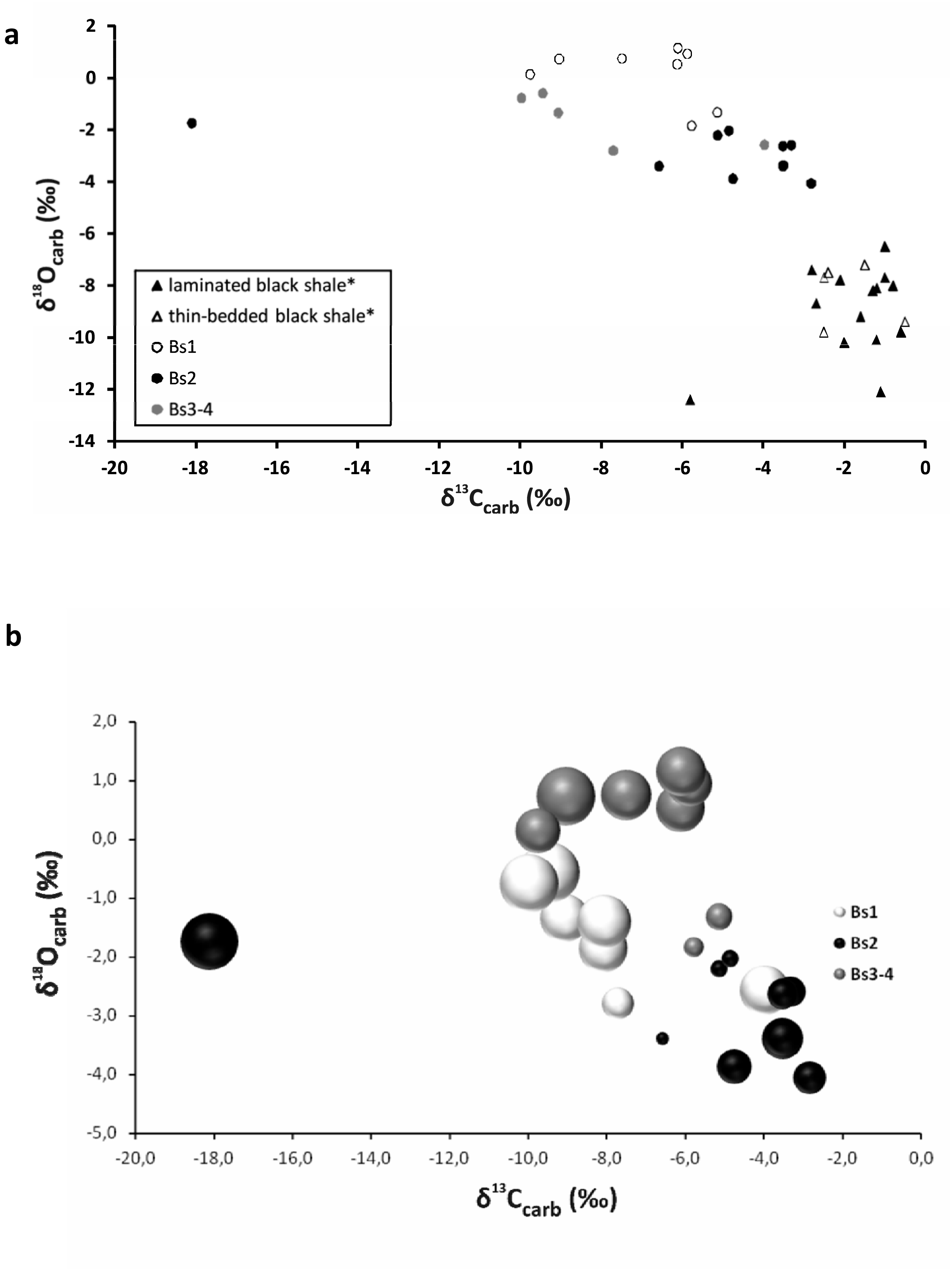
a
2
0
-2
-4
-6
-8
-10
-12
-14
-20
-18
-16
-14
-12
-10
-8
-6
-4
-2
0
$\delta^{18}O_{carb}$ (‰)
$\delta^{13}C_{carb}$ (‰)
▲ laminated black shale*
△ thin-bedded black shale*
○ Bs1
● Bs2
● Bs3-4
b
2,0
1,0
0,0
-1,0
-2,0
-3,0
-4,0
-5,0
-20,0
-18,0
-16,0
-14,0
-12,0
-10,0
-8,0
-6,0
-4,0
-2,0
0,0
$\delta^{18}O_{carb}$ (‰)
$\delta^{13}C_{carb}$ (‰)
○ Bs1
● Bs2
● Bs3-4